T2R2 東京科学大学 リサーチリポジトリ
Science Tokyo Research Repository

論文 / 著書情報
Article / Book Information

題目(和文)	透明酸化物半導体の光・電子デバイスへの応用
Title(English)	Optoelectronic device application of transparent oxide semiconductors
著者(和文)	太田裕道
Author(English)	
出典(和文)	学位:博士(工学), 学位授与機関:東京工業大学, 報告番号:甲第4915号, 授与年月日:2001年9月30日, 学位の種別:課程博士, 審査員:
Citation(English)	Degree:Doctor (Engineering), Conferring organization: Tokyo Institute of Technology, Report number:甲第4915号, Conferred date:2001/9/30, Degree Type:Course doctor, Examiner:
学位種別(和文)	博士論文
Type(English)	Doctoral Thesis

Powered by T2R2 (Science Tokyo Research Repository)

Optoelectronic Device Application of Transparent Oxide Semiconductors

HIROMICHI OHTA

Department of Innovative and Engineered Materials

Tokyo Institute of Technology

Contents

Chapter 1. 1

General introduction

1.1. Background of Present Study 1
1.1.1. Transparent Oxide Semiconductors 1
1.1.2. P-type Transparent Oxide Semiconductor, $SrCu_2O_2$ 1
1.1.3. N-type Transparent Oxide Semiconductor, ZnO 2
1.1.4. Heteroepitaxial Growth 3
1.2. Objectives and Outline of the Present Study 3
References 5

Chapter 2. 7

Highly Electrically Conductive Indium-Tin-Oxide Thin Films Epitaxially Grown on Yittria-Stabilized Zirconia (100) by Pulsed-Laser Deposition

2.1. Introduction 7
2.2. Experimental 8
2.3. Results and Discussion 9
2.4. Conclusions 11
References 12

Chapter 3. 17

Transparent Conducting Indium-Tin-Oxide Thin Film with Extremely Flatted Surface

3.1. Introduction 17
3.2. Experimental 18
3.3. Results and Discussion 19
3.4. Conclusions 22
References 24

Chapter 4. 30

Heteroepitaxial Growth of Zinc Oxide Single Crystal Thin Films on (111) Plane YSZ by Pulsed-Laser Deposition

4.1. Introduction 30
4.2. Experimental 30
4.3. Results 31
4.4. Conclusions 33
References 35

Chapter 5. 44

Electronic Structure and Optical Properties of P-Type Transparent Oxide Semiconductor; $SrCu_2O_2$

5.1. Introduction 44
5.2. Experimental 45
5.2.1. Energy Band Calculation 45
5.2.2. Bulk Ceramic Preparation and PES / IPES Measurement 45
5.2.3. Thin Film Preparation and Optical Measurement 46
5.3. Results and Discussion 47
5.3.1. Energy Band Diagram 47
5.3.2. PES / IPES Measurement 48
5.3.3. Optical Properties 49
5.4. Conclusions 50
References 52

Chapter 6. 61

Fabrication and Characterization of Ultraviolet-Emitting Diodes Composed of Transparent P-N Heterojunction, p-$SrCu_2O_2$ / n-ZnO

6.1. Introduction 61
6.2. Experimental 62
6.3. Results 64
6.3.1. Crystal Quality and Orientation of the Multilayered Films 64
6.3.2. UV-Light Emission due o Hetero P-N Junction 65
6.3.3. Visible Light Emission due to Hetero P-I-N Junction 67
6.4. Conclusions 67

References 69

Chapter 7. **82**
Summary and General Conclusions

7.1. Conclusions 82
7.2. Suggested Future Research 85
References 87

Acknowledgements 88
Publication Lists 89
Oral Presentation Lists 94

Chapter 1.
General introduction

1.1. Background of Present Study

1.1.1. Transparent Oxide Semiconductors

Transparent conductive oxides (TCOs) are widely used as transparent (metal) electrode for various displays and solar cells [1]. However, there is almost no application based on active function as a semiconductor notwithstanding that TCO is an n-type conductor. This primary reason is missing p-type TCO because most active functions in semiconductors come from the characteristic properties of pn-junction. We anticipate that new frontier of transparent oxide semiconductors (TOS) utilizing both optical transparency and electron activity in semiconductors will be opened in front of us if a p-type TCO is realized. In 1997, we reported $CuAlO_2$ (thin films) [2] as a first p-type TCO along with a chemical design concept to explore the candidate materials. After that, a series of p-type TCOs based on Cu^+ -based system have been reported following the design concept [3], i.e., $CuGaO_2$ [4], $CuInO_2$ [5] and $SrCu_2O_2$ [6].

Light Emitting Diodes (LEDs), one of optoelectronic devices, are generally composed of p-n junction using both p- and n-type semiconductors. Emission wavelength (λ) of LED is determined by band gap energy (E_g) as follows:

$$\lambda\ (\mathrm{nm}) = 1240 / E_g\ (\mathrm{eV})$$

Thus, ultraviolet emitting diode (UV-LED) would be fabricated by using transparent oxide semiconductors with larger band gap of > 3.1 eV.

1.1.2. P-type Transparent Oxide Semiconductor, $SrCu_2O_2$

$SrCu_2O_2$ was firstly found by Teske and Muller-Buschbaum in 1970 [7]. The crystal structure belongs to the $I4_1/amd$ space group. The cell parameters are a = b = 0.5469 nm, c = 0.9826 nm. It is noted that zigzag chains of O-Cu-O dumbbell-shaped structure are aligned along a- and b-axis directions ([100]). In 1998, A. Kudo et al. reported transparent p-type conductive polycrystalline thin film of $SrCu_2O_2$ grown on SiO_2 substrate at 300 °C by pulsed-laser deposition technique [6]. DC electrical conductivity of the film was 3.9 x 10^{-3} Scm^{-1} at room temperature. The band gap of the film was estimated to be 3.3 eV. Although doping of K^+ for Sr^{2+} sites increased the conductivity to 4.8 x 10^{-2} Scm^{-1}, the doping efficiency was as small as 1 %. Carrier concentration and Hall mobility of the K-doped film were 6.1 x 10^{17} cm^{-3} and 0.46 $cm^2(Vs)^{-1}$, respectively.

Thus, p-type conductive $SrCu_2O_2$ film is grown at relatively low substrate temperature of 300 °C. This is very good point to avoid interfacial reactions.

1.1.3. N-type Transparent Oxide Semiconductor, ZnO

ZnO, an n-type TOS with band gap energy of 3.37 eV, is well-known material to apply for varistors, surface acoustic wave (SAW) devices, transparent electrode, and green phosphor. ZnO is an efficient UV-emitting material (λ = 380 nm) at room temperature due to excitons, having sufficiently large binding energy (59 meV, 28 meV for GaN) to be stable even at room temperature [8]. Lasing operations using transitions associated with the exciton have been reported by electron beam [9] and UV-laser excitation [10-12]. UV-LEDs based on metal-insulator-semiconductor (MIS) junctions have been reported based on Ag/SiO/ZnO [13], Au/SiO/ZnO [14] and Cu_2O/ZnO [15]. However, no UV-emission based on p-n junctions has been realized to date, due to the

difficulty of fabricating p-type ZnO, although several attempts including laser doping [16] or co-doping [17] have been made.

1.1.4. Heteroepitaxial Growth

In 1999, A. Kudo et al. reported the realization of a p-n heterojunction composed of transparent oxide semiconductors, p-$SrCu_2O_2$ and n-ZnO that demonstrated typical electrical current rectifying behavior [18]. However no light emissions due to current injection were detected, due primarily to the poor crystallinity of the ZnO and $SrCu_2O_2$ layers grown on glass substrate. Therefore, in order to realize UV-LED composed of transparent oxide semiconductors, the diode should be fabricated by using heteroepitaxial layers of transparent oxide semiconductors.

1.2. Objectives and Outline of the Present Study

Taking the backgrounds into consideration, the target formulated in the present study is to demonstrate UV-LED entirely based on heteroepitaxially grown transparent oxide semiconductors. In order to realize this target, three objectives were given as follows:

(1) Heteroepitaxial growth and characterization of transparent oxide semiconductors, ITO and ZnO.

(2) Observation of electronic structure of p-type transparent oxide semiconductor, $SrCu_2O_2$

(3) Fabrication and characterization of UV-LED composed of p-n heterojunction of p-$SrCu_2O_2$ and n-ZnO

In chapter 2-4, high quality ITO and ZnO thin films were grown hetero-epitaxially on extremely flat substrate of YSZ by a pulsed laser deposition technique, and crystallinity, optical and electrical properties of these films were investigated.

In chapter 5, the electronic structure of wide gap (~3.3 eV) p-type oxide semiconductor, $SrCu_2O_2$, is examined by photoelectron (UPS, XPS and IPES) and optical spectroscopy (absorption and emission), and results obtained are compared with energy band structure calculated by local density approximation method to clarify the origin of p-type conductivity in this material.

In chapter 6, UV light emitting diode operating at room temperature was realized using a hetero p-n junction composed of transparent conductive oxides, p-$SrCu_2O_2$ and n-ZnO. A rather sharp emission band centered at 382 nm was generated when the forward bias voltage exceeding turn-on voltage of 3 V was applied to the junction. The emission may be attributed to a transition associated with electron hole plasma of ZnO.

In chapter 7, the present study is summarized.

References

[1] TCO special issue, *MRS Bull*, August 2000, Vol.25, No.8.

[2] H. Kawazoe, M. Yasukawa, H. Hyodou, M. Kurita, H. Yanagi and H.hosono, *Nature (London)* **389**, 939 (1997).

[3] H. Kawazoe, H. Yanagi, K. Ueda and H. Hosono, *MRS Bull.* **25**, 28 (2000).

[4] K. Ueda, T. Hase, H. Yanagi, H. Kawazoe, H. Hosono, H. Ohta, M. Orita and M. Hirano, *J. Appl. Phys.* **89**, 1790 (2001).

[5] H. Yanagi, T. Hase, S. Ibuki, K. Ueda and H. Hosono, *Appl. Phys. Lett.* **78**, 1583 (2001).

[6] A. Kudo, H. Yanagi, H. Hosono and H. Kawazoe, *Appl. Phys. Lett.* **73**, 220 (1998).

[7] L. Teske and Hk. Muller-Buschbaum, *Z. Anorg. Allg. Chemie.* **379**, 113 (1970).

[8] D. G. Thomas, *J. Phys. Chem. Solids* **15**, 86 (1960).

[9] F. H. Nicoll, *Appl. Phys. Lett.* **9**, 13 (1966).

[10] D. C. Reynolds, D. C. Look and B. Jogai, *Solid State Commun.* **99**, 873 (1996).

[11] D. M. Bagnall, Y. F. Chen, T. Yao, S. Koyama, M. Y. Shen and T. Goto, *Appl. Phys. Lett.* **70**, 2230 (1997).

[12] P. Zu, Z. K. Tang, G. K. L. Wong, M. Kawasaki, A. Ohtomo, H. Koinuma and Y. Segawa, *Solid State Commun.* **103**, 459 (1997).

[13] B. W. Thomas and D. Walsh, *Electronics Lett.* **9**, 362 (1973).

[14] T. Minami, M. Tanigawa, M. Yamanishi and T. Kawamura, *Jpn. J. Appl. Phys.* **13**, 1475 (1974).

[15] I. T. Drapak, *Soviet Phys. Semiconductors* **2**, 513 (1968). (The electro-luminescence from Cu_2O/ZnO was stated from p-n junction. However, judging from high bias voltage required for the emission, it has been rather considered to be

due to insulator-semiconductor junction.)

[16]T. Aoki, Y. Hatanaka and D. C. Look, *Appl. Phys. Lett.* **76**, 3257 (2000).

[17]M. Joseph, H. Tabata and T. Kawai, Jpn. *J. Appl. Phys.* **38**, L1205 (1999).

[18]A. Kudo, H. Yanagi, K. Ueda, H. Hosono, and H. Kawazoe, *Appl. Phys. Lett.* **75**, 2851 (1999).

Chapter 2.
Highly Electrically Conductive Indium-Tin-Oxide Thin Films Epitaxially Grown on Yttria-Stabilized Zirconia (100) by Pulsed-Laser Deposition

2.1. Introduction

Transparent Conducting Oxides (TCOs) have been widely used as transparent electrodes for flat panel displays, including liquid crystal displays (LCDs), organic LEDs, and plasma displays. Among the thin-film materials commonly used, tin-doped In_2O_3 (ITO) is preferred, especially for LCDs, due to its lower electrical resistivity and compatibility with fine patterning processes. Commercial ITO films have been mainly produced by DC magnetron sputtering methods, and tremendous efforts have been expended in bringing their resistivities down to around 2×10^{-4} Ωcm by restraining the bias voltage [1]. However, recent demands for larger LCDs with more precise patterns will require resistivity to be decreased below 1×10^{-4} Ωcm, a goal unlikely to be realized by sputtering methods.

Resistivity can be improved by increasing electron mobility and/or carrier density. Although there is a trade-off between these two parameters, mobility enhancement is the more favorable alternative for TCO films due to their higher carrier density, especially when it exceeds more than 2×10^{21} cm^{-3}, which causes strong optical absorption due to the plasma excitation of the carrier in the visible range. Several attempts have been made to decrease the resisitivity through mobility enhancement by employing novel deposition techniques such as electron-beam evaporation [2] and pulsed-laser deposition (PLD) [3-8], or by using appropriate crystalline substrates [2-4,9]. As examples of the latter technique, several papers have reported the use of an

yttria-stabilized zirconia (YSZ, lattice type; cubic) substrate for ITO film growth, since the mismatch between the lattice constant of the a-axis of ITO, twice that of YSZ, is less than 1.6% [2,5,9]. However, the resistivity of the films obtained so far have not been sufficiently low, nor has the crystal quality been so good. We expected that effective enhancement of film quality could be achieved by epitaxial crystalline growth using an extremely flat surface at a relatively high substrate temperature. Here, we report the fabrication of highly electrically conductive ITO thin films by epitaxial growth on an extremely flat surface of YSZ single crystal using PLD and a substrate temperature of 600°C.

2.2. Experimental

It was found after a series of experiments that the annealing temperature was the most effective parameter for preparing the extremely flat YSZ (100) substrates required. Commercially available synthetic YSZ (100) single-crystal substrates were heated in air at 1350°C to obtain an atomically flat YSZ surface. The terraced and stepped structure of the substrate surface was clearly observed by AFM (SII SPI-3700). Terrace widths were about 150 nm, and step height was 0.26 nm agreeing well with the separation between adjacent (200) planes of the YSZ crystals (0.257 nm). These flat-surface YSZ single crystals served as substrates for ITO film growth by PLD. Background pressure of the deposition chamber was 2 x 10^{-6} Pa, and the oxygen gas pressure was kept at 1.2 x 10^{-3} Pa during deposition. A KrF excimer laser beam (wavelength, 248 nm; pulse duration, about 20 ns; repetition frequency, 10 Hz) was focused through a SiO_2 glass window onto a rotating ITO ceramic target to produce a photon power density of about 6J/cm^2/pulse. The substrate, facing the target, was rotated mechanically and maintained

at 600°C during deposition.

Crystalline quality and orientation were analyzed by X-ray diffraction (ATX-G, Rigaku Co.), measured with the ω axis rotated in the horizontal plane and the ϕ axis rotated azimuthally. The detector was manipulated with the 2θ axis in the horizontal plane and $2\theta\chi$ axis in the vertical plane, respectively. Crystal orientation was measured by simultaneous scans of the 2θ and ω axes. Sample crystal quality was analyzed from measurements of 2θ-fixed ω-scanning (out-of-plane rocking curve). Diffraction analysis for the lattice planes perpendicular to the film-substrate interface, which effectively reveals the lateral structure of the thin film, was performed with $2\theta\chi$-fixed ϕ-scans (in-plane rocking curve).

2.3. Results and Discussion

Figure 2-1(a) shows the ω-2θ patterns of films deposited on YSZ (100). Only intense peaks diffracted from the (h00) plane of the film, along with those from the YSZ substrate, are observable. Such good preferential orientation is not seen in the XRD pattern of thin films deposited on a SiO_2 glass substrate shown in Fig. 2-1(b). The full width at half maximum of the diffraction peak in the out-of-plane rocking curve of (400) ITO in Fig. 2-1(c) was about 0.4 degree, indicating an excellent orientation of $(h00)_{ITO}//(100)_{YSZ}$. Four-fold symmetry is clear in the in-plane rocking curve shown in Fig. 2-1(d), which is in excellent agreement with the case $(h00)_{ITO}$ // $(100)_{YSZ}$ & $(0h0)_{ITO}$ // $(0h0)_{YSZ}$. This data reveals that the ITO thin films deposited on the YSZ substrate are epitaxially grown, keeping an orientation $(h00)_{ITO}$ // $(h00)_{YSZ}$ and $(0h0)_{ITO}$ // $(0h0)_{YSZ}$. The cross-sectional TEM (JEM-2000EX, JEOL) image of Fig. 2-2 substantiates this conclusion. Although several misfit dislocations and edge dislocations are seen, the

interface may be regarded as being smoothly connected, proving that hetero-epitaxial growth occurs.

Figure 2-3 summarizes the electrical resistivity (a), Hall mobility (b), and the carrier density (c) for ITO/YSZ (open circles) and ITO/SiO_2 films (solid circles) as a function of SnO_2 concentration in the films. The electrical properties were measured by a conventional van der Pauw method, and the concentration was analyzed by XRF measurement (RIX2100, Rigaku). Better performance was obtained for ITO/YSZ than for ITO/SiO_2 for each parameter in almost the entire concentration region. The electrical resistivity of ITO/YSZ decreases sharply from about 10^{-2} Ωcm to below 10^{-4} Ωcm with doping of SnO_2, and it saturates when SnO_2 exceeds 3 wt.%, showing a gentle peak at 5.7 wt% SnO_2. Corresponding to this behavior, the carrier density increases rapidly with an increase in the SnO_2 concentration initially, and it also saturates with a further increase. On the other hand, the mobility shows a slight decrease almost linearly with the concentration, but the slope of the reduction was fairly moderate compared to that in conventional ITO films. The lowest resistivity of 7.7 x 10^{-5} Ωcm was obtained in the film containing 5.7 wt.% SnO_2, in which the mobility was 42 $cm^2V^{-1}s^{-1}$ and the carrier density was 1.9 x 10^{21} cm^{-3}. This value of resistivity is among the lowest ever reported, except for that of an ITO film with a non-homogeneous structure of tin concentration [10]. These observations lead to the conclusion that the low resistivity of the ITO/YSZ films is due to the larger mobility and the slight decrease with SnO_2 concentration, in spite of the rapid increase in carrier density. It is further considered that the large mobility is most likely to have resulted from the good crystal quality of the films.

Figure 2-4 shows the optical transmission (T) and the reflection spectra (R) in the visible and near-IR region for the ITO/YSZ film containing 5.7 wt.% SnO_2 (lowest

resistivity specimen). In this figure, transmission and reflection due to the YSZ substrate are also shown by dotted lines for comparison. More than 85% of visible light is transmitted through the film.

2.4. Conclusions

In summary, we have succeeded in reproducible fabrication of low resistivity ITO films (as low as 7.7×10^{-5} Ωcm) by epitaxial growth on an extremely flat YSZ (100) substrate by PLD. The lowest resistivity was obtained in a film containing 5.7 wt.% SnO_2. The low resistivity originates from the specimen's large electron mobility, which most likely resulted from the good crystal quality of the films. The optical transmissivity of the film exceeded 85% at wavelengths from 340 nm to 780 nm.

Acknowledgements

The authors thank Dr. K. Inaba and Mr. T. Nakatani of Rigaku Corporation for the XRD and XRF measurements, and Ms. M. Yuuki of the HOYA Corporation for the TEM observation.

References

[1] S. Ishibashi, Y. Higuchi, Y. Ota and K. Nakaumura, *J. Vac. Sci. & Technol.* **A8,** 1403 (1990).

[2] N. Taga, H. Odaka, Y. Shigesato, I. Yasui, M. Kamei and T. E. Haynes, *J. Appl. Phys.* **80**, 978 (1996).

[3] E. J. Tarsa, J. H. English and J. S. Speck, *Appl. Phys. Lett.* **62**, 2332 (1993).

[4] Q.X. Jia, J.P. Zheng, H.S. Kwok and W.A. Anderson, *Thin Solid Films* **258**, 260 (1995).

[5] C. Coutal, A. Azema and J.C. Roustan, *Thin Solid Films* **288**, 248 (1996).

[6] F. O. Adurodija, H. Izumi, T. Ishihara, H. Yoshioka, K. Yamada, H. Matsui and M. Motoyama, *Thin Solid Films* **350**, 79 (1999).

[7] H. Kim, A. Pique, J.S. Horwitz, H. Mattoussi, H. Murata, Z.H. Kafafi and D.B. Chrisey, *Appl. Phys. Lett.* **74**, 3444 (1999).

[8] Y. Wu, C.H.M. Maree, R.F. Haglund, Jr., J.D. Hamilton, M.A. Morales Paliza and R.A. Weller, *J. Appl. Phys.* **86**, 991 (1999).

[9] M. Kamei, T. Yanagi, S. Takaki and Y. Shigesato, *Appl. Phys. Lett.* **64**, 2712 (1994).

[10] I.A. Rauf, *J. Mater. Sci. Lett.* **12**, 1902 (1993).

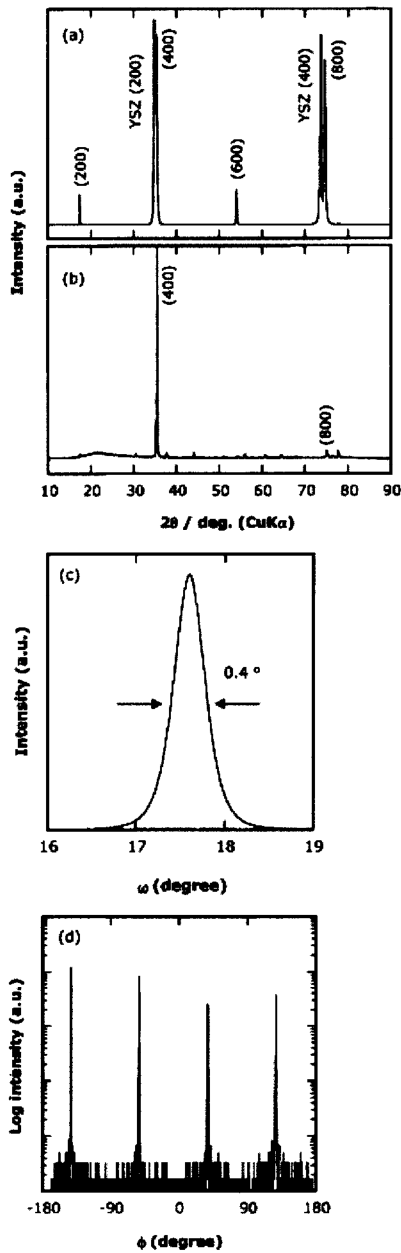

Figure 2-1. X-ray diffraction patterns of ITO thin films. (a) ω-2θ scans for films deposited on YSZ (100) surface and (b) deposited on SiO_2 glass. (c) out-of plane rocking curves (ω-scan) of (400) ITO deposited on YSZ (100). (d) in-plane rocking curve (ϕ– scan).

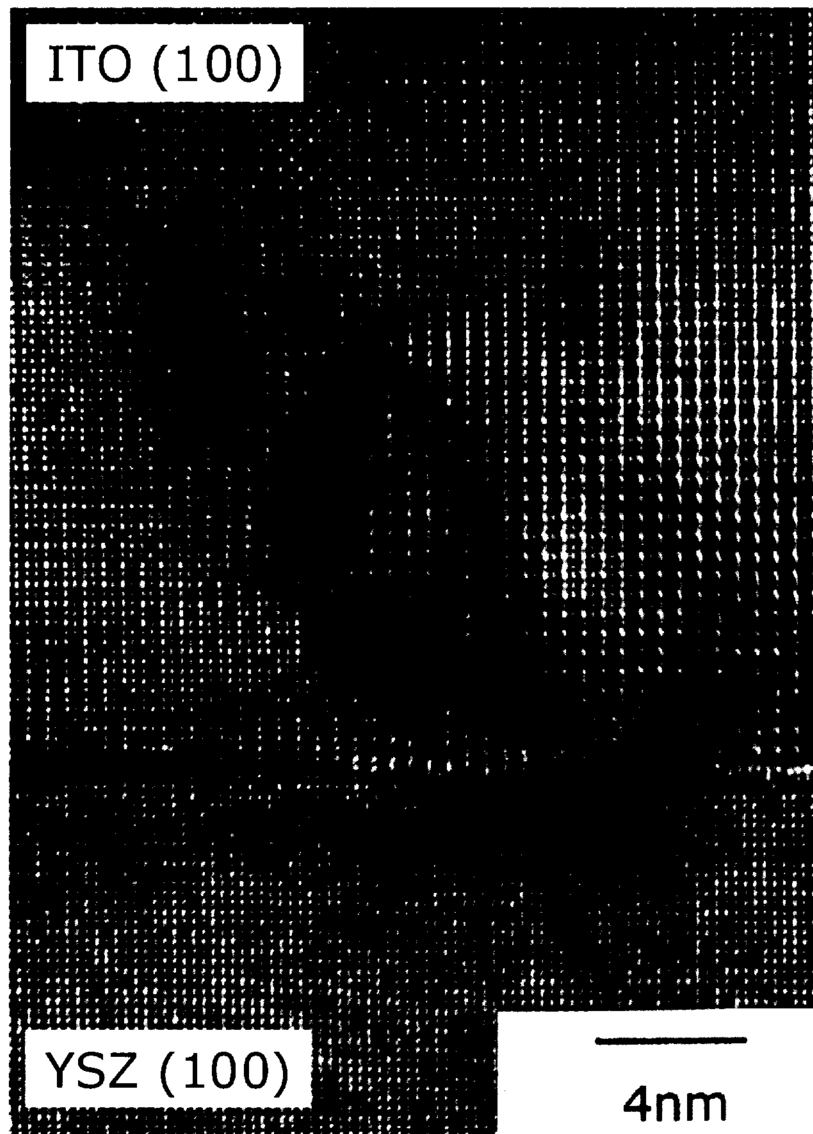

Figure 2-2. Cross-sectional TEM photograph of ITO/YSZ interface. Electron-beam incidence was <100> on YSZ. The interface may be regarded as being smoothly connected, proving that heteroepitaxial growth occurs.

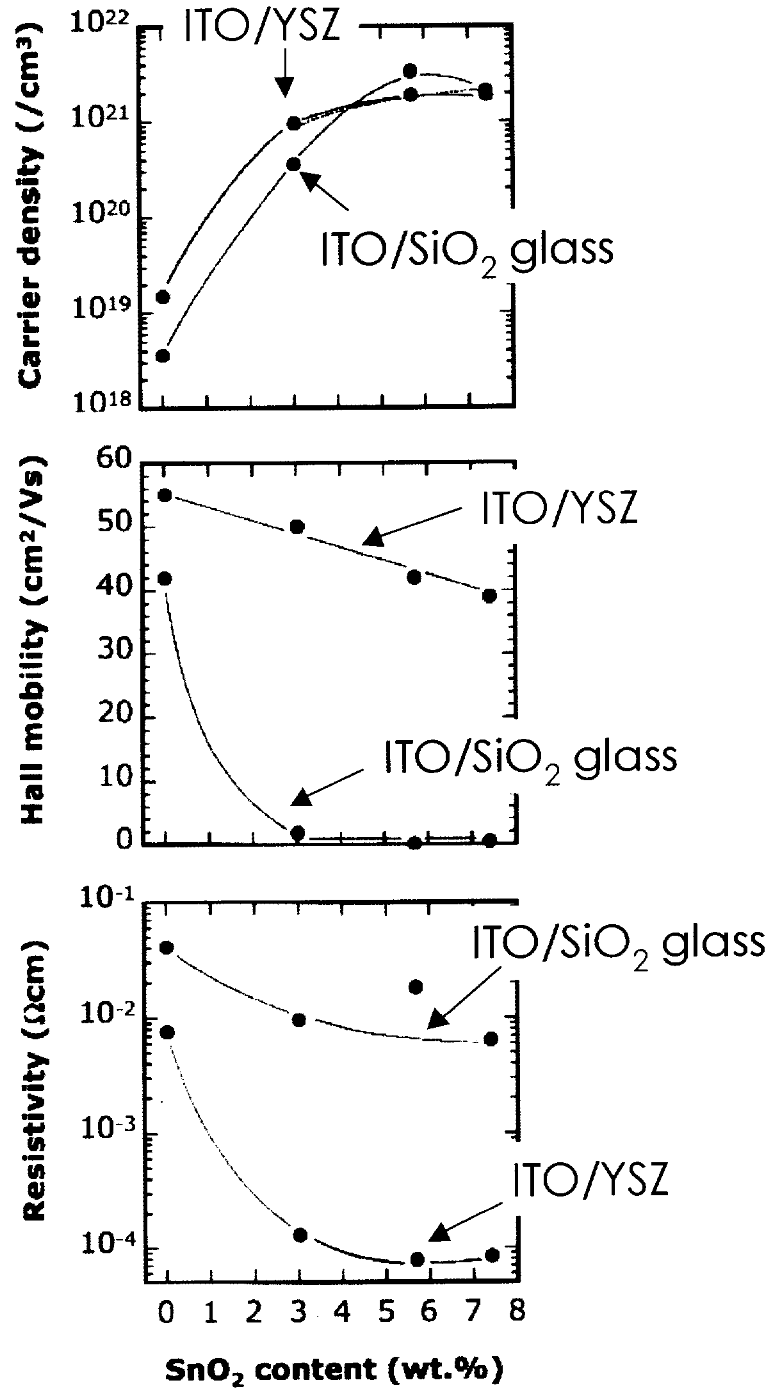

Figure 2-3. Resisitivity, Hall mobility, and carrier density of ITO thin films deposited on YSZ (100) as a function of SnO_2 film content. [●: ITO/YSZ, ●: ITO/SiO_2 glass]

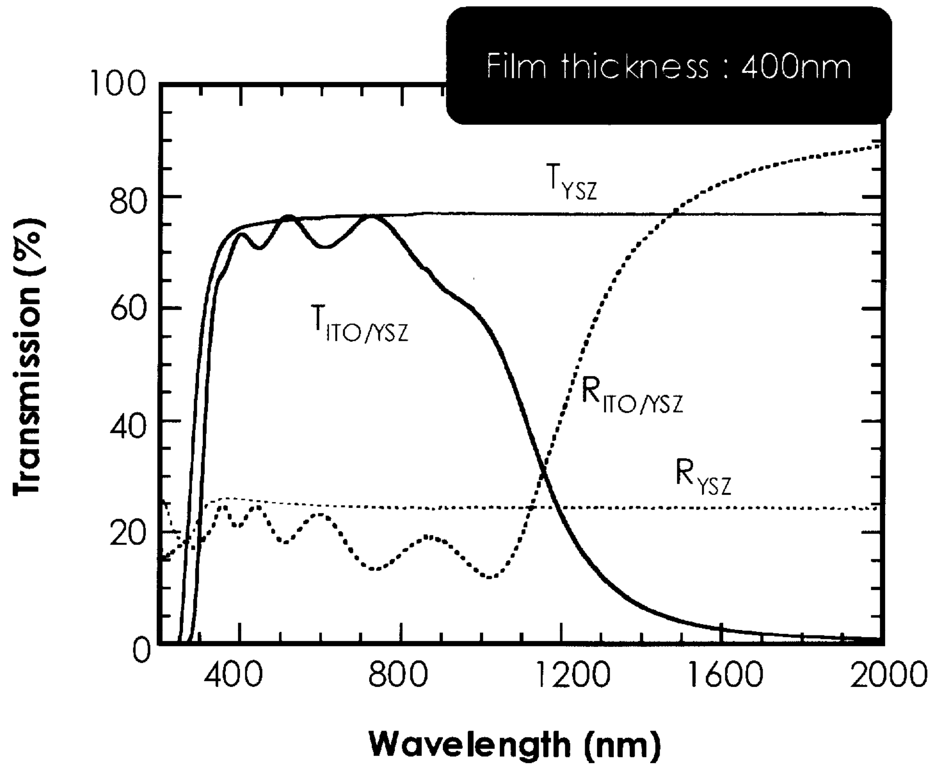

Figure 2-4. Optical transmission and reflection spectra of ITO (SnO_2: 5.7 wt.%) thin film deposited on YSZ (100). Film thickness was about 400 nm. Those of the YSZ (100) substrate are also shown for comparison.

Chapter 3.
Transparent Conducting Indium-Tin-Oxide Thin Film with Extremely Flatted Surface

3.1. Introduction

Tin-doped indium oxide (ITO) with C-rare earth crystal structure (Crystal system: cubic, Space group: Ia_3, a_0=1.0118 nm (In_2O_3)) is widely applied as transparent electrode for flat panel displays such as liquid crystal displays (LCDs) and solar cells [1]. Recently, ITO films have also been used as cathode electrodes for UV-emitting diodes, in which the ITO film acts as a cladding layer, substrate for n-type conductive layers and electrode [2]. For use in such optoelectronic device application, device properties would depend sensitively on the surface morphologies and crystal quality of ITO film. Further, transparent conductive ITO films with atomically flat surface could be used as substrates for a modified scanning tunneling microscope (STM) to measure simultaneously STM image and luminescence from very local area of organic or bio materials such as DNA and dye molecules [3].

An important aspect in understanding the surface morphology and crystal quality of ITO film is to study the film growth mechanisms on single crystal substrate. Yittria-stabilized-zirconia (YSZ) with fluorite crystal structure (Crystal system: cubic, Space group: Fm3m, a_0=0.5139 nm ($Y_{0.15}Zr_{0.85}O_{1.93}$)) is preferred substrate material for heteroepitaxial growth of ITO film due primary to similar crystal structure. Lattice mismatch between a unit cell of ITO and two unit cells of YSZ is less than 1.6 % [2, 4-7]. We recently reported that highly electrical conductive ITO thin films with resistivity of less than 1×10^{-4} Ωcm may be grown heteroepitaxially on a single crystal of YSZ (100) surface by a pulsed-laser deposition (PLD) technique [7]. Large grains with 100 -

200 nm diameters were observed, which would indicate typical columnar growth.

We have attempted three types of approaches to further improving the surface morphology of heteroepitaxial ITO film. First, ITO thin films were grown at higher temperatures to enhance surface diffusion of deposited atoms, with an intention to change the growth mode from columnar growth to spiral and/or step flow growth. Second, two different (111) and (100) surfaces of YSZ were used for ITO film growth. YSZ cleaves readily along (111) planes. Thus, one would expect that atomic migration of relevant ions on the (111) plane would be enhanced markedly compared to that on the (100) plane of YSZ. Finally, ITO films were grown in various oxygen pressures. In general, oxygen pressure during oxide film growth effects on crystallinity and surface morphology [8], because kinetic energy of atoms or clusters deposited at the surface may differ depending on the oxygen pressure, which in turn changes the growth rate of the oxide film. Here, we report on the surface morphology and crystal quality of ITO film grown heteroepitaxially on YSZ (111) and (100) substrate using a PLD technique at a substrate temperature of 900 °C for various oxygen gas pressures.

3.2. Experimental

YSZ (111) and (100) substrates were annealed at 1350 °C in air to obtain atomically flat surface [7]. Annealed YSZ single crystal plates were used as substrates for ITO film grown by a PLD technique. An atomically flat substrate surface is essential for the observation of surface morphology with an atomic scale resolution. The background pressure of the growth chamber was 2×10^{-6} Pa, while the oxygen pressure during the growth was fixed in the range form 2×10^{1} to 2.2×10^{-3} Pa. A KrF excimer laser beam (λ = 248 nm; pulse duration = 20 ns; repetition frequency = 10 Hz) was

focused through a SiO_2 glass window onto a rotating ITO ceramic target (In_2O_3 : SnO_2 (10 wt.%)) to produce a photon energy density of 2 J/cm^2/pulse. Facing the target, the substrate was rotated mechanically and maintained at 900 °C during film growth.

Crystal quality and orientation were analyzed by high-resolution X-ray diffraction measurements (HR-XRD, ATX-G, Rigaku Co.). The out-of-plane XRD pattern (synchronous scan of 2θ and ω in the horizontal plane), in-plane XRD pattern (synchronous scan of $2\theta\chi$ and ϕ in the azimuth plane), out-of-plane rocking curve (OXRC, 2θ fixed ω scan) and in-plane rocking curve (IXRC, $2\theta\chi$ fixed ϕ scan) were obtained. Surface morphology was observed by using an atomic force microscope (AFM, SPI-3700, S.I.I.). Electrical properties of the ITO thin films were measured by van der Pauw method at room temperature.

3.3. Results and Discussion

Typical electrical resistivity, the carrier density, and Hall mobility of the ITO thin films grown on (111) YSZ surface at a substrate temperature of 900 °C and the oxygen pressure of 2.2 x 10^{-3} Pa were $\sim$1 x 10^{-4} Ωcm, $\sim$1.5 x 10^{21} cm^{-3}, and $\sim$50 cm^2(Vs)$^{-1}$, respectively.

Figure 3-1(a) and (b) show out-of-plane XRD patterns of ITO film grown on (a) (111) YSZ and (b) (100) YSZ, respectively. Only intense peaks of (222) ITO together with (111) YSZ and (400) ITO together with (200) YSZ were observed respectively in out-of-plane XRD patterns, indicating a mutual crystal orientation relationship of (a) ITO (111) // YSZ (111) and (b) ITO (100) // YSZ (100). Pendelloesung fringes, indicating good crystal quality and flat surface, are clearly seen in Fig. 3-1 (a). Such fringes are not seen in Fig. 3-1 (b). Figure 3-1 (c) and (d) show the OXRCs of (c) ITO

(111) shown in Fig. 3-1 (a) and (d) ITO (100) shown in Fig. 3-1 (b), respectively. The full-width at half-maximum (FWHM) of the OXRC of (222) ITO on (111) YSZ shown in Fig. 3-1 (c) is 0.015 degree (54 arcsec.), corresponding to the very small tilting of the film. The value is the smallest reported in the literature to date [4-6]. A broad tail component of the rocking curve also appears in Fig. 3-1 (c). The presence of edge dislocations and/or screw dislocations is tentatively ascribed to the origin of this component. Such small crystal tilting is not seen in the OXRC of ITO films grown on (100) YSZ shown in Fig. 3-1 (d). In-plane XRD measurements were also performed around a critical angle of the X-ray total external reflection. Figure 3-2 shows IXRCs of (110) ITO (a) and (010) ITO (b). Six-fold (a) and four-fold (b) symmetries were clearly seen in Fig. 3-2. These results suggest that heteroepitaxial growth in both lateral and vertical directions occurred in each case of ITO on YSZ.

Figure 3-3 shows AFM images (1 x 1 μm^2) of ITO films grown heteroepitaxially on (a) YSZ (111) and (b) YSZ (100) surfaces at 900 °C with the oxygen pressure of 2.2 x 10^{-3} Pa. Circular or hexagonal 3D spiral structures, composed of atomically flat terraces with a width of 50 - 150 nm and steps, were observed. The step increments were - 0.3 nm as seen in cross sectional line profile, agreeing well with the distance between two adjacent (222) planes of ITO (0.291 nm; measured by HR-XRD). This observation indicates that films grow in a 3D-spiral growth mode on YSZ (111). On the other hand, surface of the film grown on (100) exhibits large roughness, covered with rectangle structures and no spiral is seen as shown in Fig. 3-3 (b), suggesting that the crystal growth on (100) surface is of columnar growth mode. The difference in the growth mode suggests that the migration rate of deposited atoms on YSZ (111) is greater than that on YSZ (100).

Figure 3-4 show AFM images (1 x 1 μm^2) of ITO film hetero-epitaxially grown on YSZ (111) surface at 900 °C in various oxygen pressures of 2.2 x 10^{-3} Pa (a), 1.0 x 10^{-1} Pa (b), and 2 x 10^{1} Pa (c), respectively. The growth rates of ITO films were (a) 2, (b) 1.5, and (c) 0.05 nm/s, respectively. That is, an increase in the growth rate is confirmed when decreasing the oxygen gas pressure. 3D-spiral grains with 1 μm in diameter were seen in Fig. 3-4 (a). The grain diameter became smaller to 100 - 200 nm in Fig. 3-4 (b) and it further decreased with increasing oxygen pressure. Finally, as shown in Fig. 3-4 (c), nearly straight terrace structure with a width of 50 - 100 nm edged by waved line were observed without 3D-spiral structures. The structure suggests us to consider as if the growth mode would change from spiral to 2D step-flow modes. However, this consideration is denied by the observation that the terrace width of YSZ (111) substrate (200 nm) is much larger than that of the film (50 - 100 nm), since the terrace width should be corresponded to that of substrate in 2D step-flow growth. The observed terrace structure is likely formed as a result of the gathering of very small 3D-spiral grains nucleated at many points on terraces of the substrate, which grows larger without migration until connected with neighboring grains. That is, ITO is basically grown on YSZ (111) by 3D-spiral growth mode and the grain size is decreased with increasing oxygen pressure during ITO film growth. Kinetic energy of the deposited atoms during film growth should be decreased with increasing oxygen pressure, which suppresses the atom migration and decreases film growth rate of ITO. Therefore, oxygen pressure during film growth is a key factor to control the film growth rate, leading to the improvement of overall surface roughness as shown in Fig. 3-4 (c).

The overall surface roughness of the ITO thin film can be evaluated by grazing-incidence X-ray reflectivity (GIXR) [9-10]. Figure 3-5 shows the GIXR pattern of an

ITO thin film grown at the same condition as that of the sample shown in Fig. 3-4 (c). (circle : measured pattern, solid line : simulated pattern). The analyzed area was 9.5 x 10 mm^2 at incident angle of the X-ray total external reflection. Kiessig fringe [9] was clearly seen in the measured pattern in Fig. 3-5. A simulation of the GIXR was conducted by a non-linear least square method according to Parratt's equation [11-12]. In this simulation, the root mean square roughness (Rms) of the film surface is treated as a fitting parameter, while measured values are used for other parameters such as film thickness (58.5 nm), film density (7.172 gcm^{-3}), and substrate surface Rms (0.1 nm). A simulated pattern exhibited good agreement with the measured pattern when the Rms of the film surface was 0.15 nm, agreeing well with the value (0.16 nm) calculated from the AFM image (proved area = 1 μm^2). This result indicates the excellent homogeneity of the film thickness over the entire film.

3.4. Conclusions

We have investigated the surface morphology and crystal quality of very low resistive (resistivity: $\sim$1 x 10^{-4} Ωcm) indium-tin-oxide films grown heteroepitaxially on YSZ surfaces at a substrate temperature of 900 °C by using high-resolution X-ray diffraction and atomic force microscope. ITO (111) films grown on (111) surface of YSZ exhibited higher crystal quality compare to ITO (100) films grown on YSZ (100), judging from the fact that the full width at half maximum of out-of-plane X-ray rocking curves of ITO (111) and ITO (400) were 54 and 720 arcsecond, respectively. The ITO (111) was grown spirally with flat terraces and steps corresponding to (222) plane spacing of 0.29 nm, while only columnar structure was observed in the ITO (100) film. ITO film was basically grown on YSZ (111) by 3D-spiral growth mode and the grain

size was decreased with increasing oxygen pressure during ITO film growth to improve overall surface roughness. In addition to higher growth temperature, cleaved surface and oxygen pressure are key factors to fabricate ITO thin film with atomically flat surface. The ITO films, simultaneously realizing distinct features including electric conductive, transparent and atomically flat surface, could open up emerging applications such as the modified STM.

References

[1] I. Hamberg and C. G. Granqvist, *J. Appl. Phys.* **60**, R123 (1986).

[2] H. Ohta, K. Kawamura, M. Orita, N. Sarukura, M. Hirano and H. Hosono, *Electronics Letters*, **36**, 984 (2000).; *Appl. Phys. Lett.* **77**, 475 (2000).

[3] R. W. Owens and D. A. Smith, *Langmuir* **16**, 562 (2000).

[4] E. J. Tarsa, J. H. English and J. S. Speck, *Appl. Phys. Lett.* **62**, 2332 (1993).

[5] M. Kamei, T. Yanagi, S. Takaki and Y. Shigesato, *Appl. Phys. Lett.* **64**, 2712 (1994).

[6] N. Taga, H. Odaka, Y. Shigesato, I. Yasui, M. Kamei and T. E. Haynes, *Jpn. J. Appl. Phys.* **37**, 6524 (1998).

[7] H. Ohta, M. Orita, M. Hirano, H. Tanji, H. Kawazoe and H. Hosono, *Appl. Phys. Lett.* **76**, 2740 (2000).; *Mat. Res. Soc. Symp. Proc.*, Vol. 623, 253 (2000).

[8] S. Choopun, R. D. Vispute, W. Noch, A. Balsamo, R. P. SHarma, T. Venkatesan, A. Iliadis and D. C. Look, *Appl. Phys. Lett.* **75**, 3947 (1999).

[9] Kiessig, *Annalen der Physik* **10**, 771 (1931).

[10] S. Wei, B. Li, T. Fujimoto and I. Kojima, *Phys. Rev.* **B58**, 3605 (1998).

[11] L. G. Parratt, *Phys. Rev.* **95**, 359 (1954).

[12] S. K. Sinha, E. B. Sirota and S. Garoff, *Phys. Rev.* **B38**, 2297 (1988).

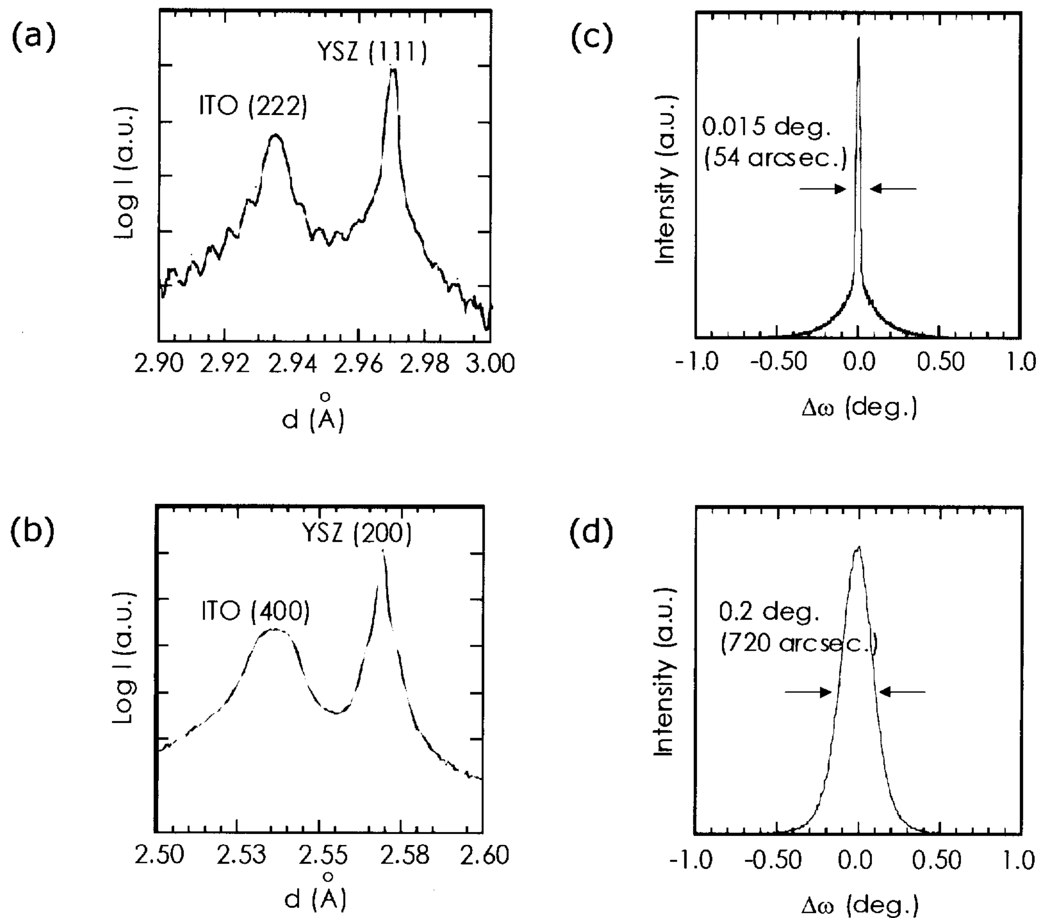

Figure 3-1. Out-of-plane XRD patterns of ITO film grown on (a) YSZ (111) and (b) YSZ (100) surfaces at a substrate temperature of 900 °C. Pendelloesung fringes are clearly seen in Fig. 1 (a). Fig. 1 (c) and (d) are the OXRC of (c) ITO (222) shown in (a) and (d) ITO (400) shown in (b).

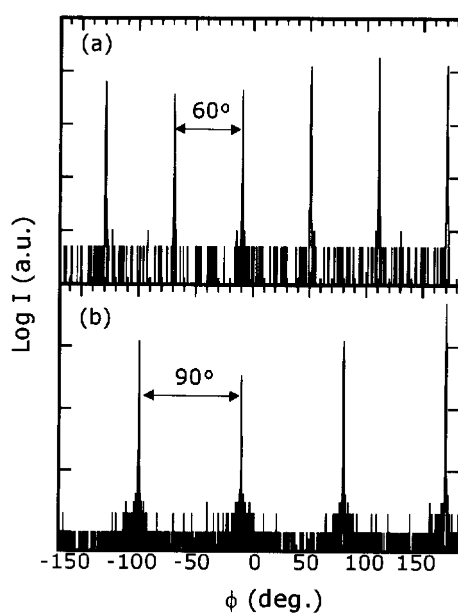

Figure 3-2. In-plane XRD rocking curves of ITO thin film grown on (a) YSZ (111) and (b) YSZ (100) surfaces at a substrate temperature of 900 °C. Six-fold symmetry every 60 degree (a) and four-fold symmetry every 90 degree (b) are seen.

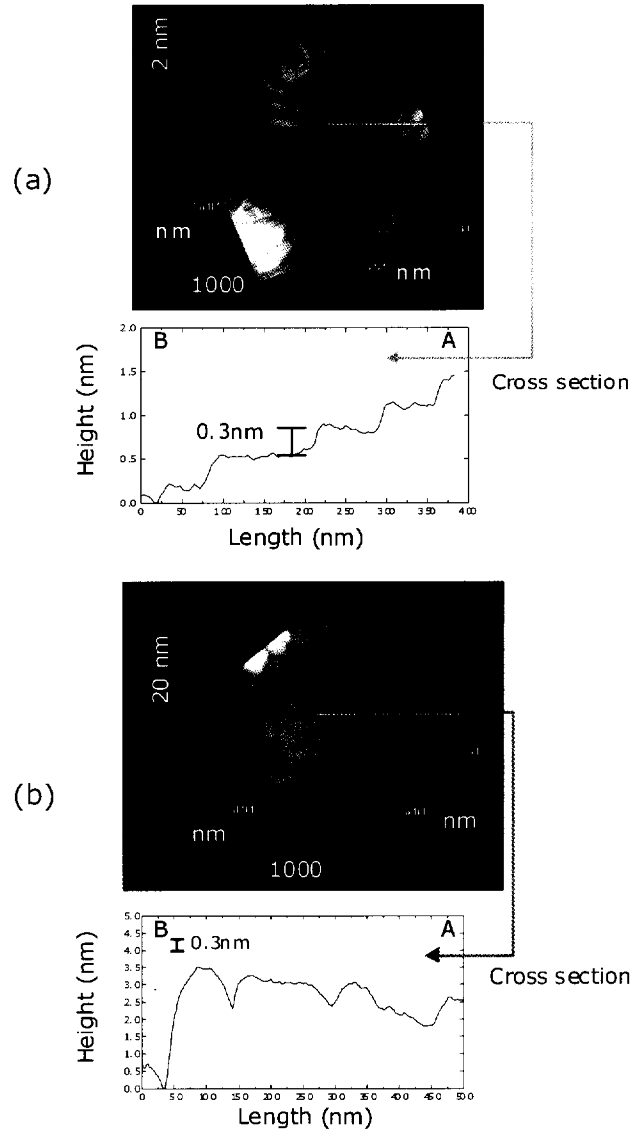

Figure 3-3. AFM images of ITO thin films grown on YSZ surface at 900 °C and their cross sectional profile [(a) ITO (111) on YSZ (111) and (b) ITO (100) on YSZ (100)]. The film thicknesses are (a) 430 nm and (b) 460 nm, respectively.

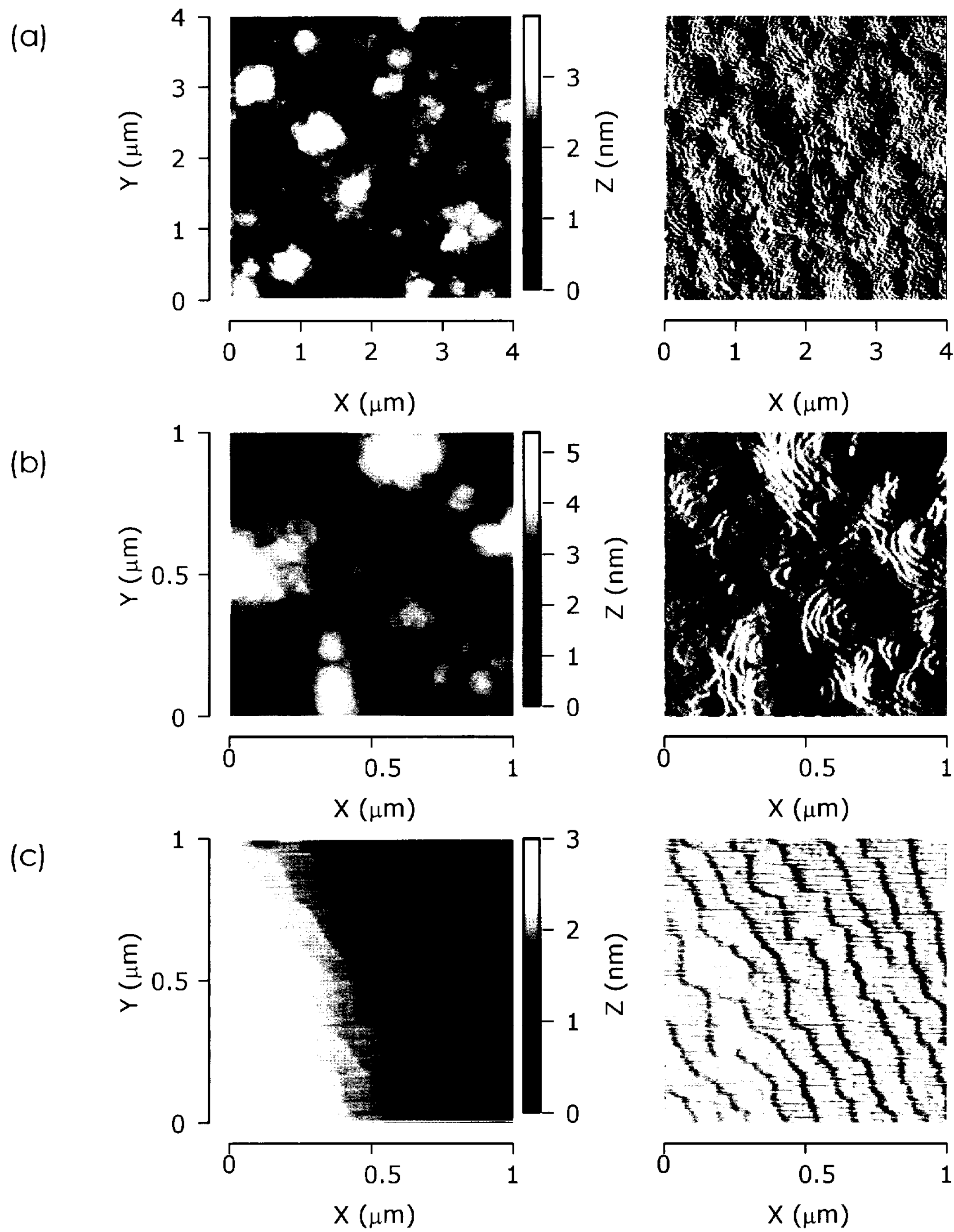

Figure 3-4. AFM images of ITO thin films grown on YSZ surface at 900 °C in various oxygen pressures during film growth. (a) 2.2 x 10^{-3} Pa, (b) 1.0 x 10^{-1} Pa and (c) 2.0 x 10^{1} Pa. (Right) Topographic and (Left) embossed image.

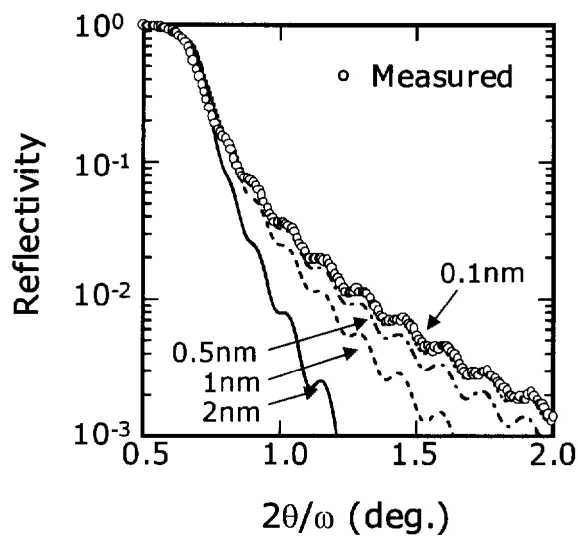

Figure 3-5. GIXR pattern of the ITO thin film grown on YSZ (111) surface at 900 °C. The film thickness is 58.5 nm. (Circle: observed, Line: Simulated)

Chapter 4.
Heteroepitaxial Growth of Zinc Oxide Single Crystal Thin Films on (111) Plane YSZ by Pulsed-Laser Deposition

4.1. Introduction

Oxide thin films with low electrical resistivity and high optical transparency in the ultraviolet to visible range have been applied to transparent electrodes for liquid crystal displays, solar cells and similar applications. Although tin doped indium oxide (ITO) is utilized in the devices, zinc oxide (ZnO) is a promising candidate material for replacing ITO in same applications because of its merits such as easy fabrication, easy etching for patterning, low cost, and rich natural resources. ZnO is a wide and direct band gap II-VI semiconductor which has an energy gap of 3.37 eV at room temperature.

The electric properties of heteroepitaxial ZnO have been investigated by several researchers. Jonson et al. reported the Hall mobility and carrier density of ZnO epilayer deposited by molecular beam epitaxy (MBE) on sapphire (0001) and on 6H-SiC, finding a ZnO / sapphire value of 34.2 cm^2/Vs and 2.6 x 10^{19} cm^{-3}, and ZnO / 6H-SiC value of 260 cm^2/Vs and 9 x 10^{18} cm^{-3}, respectively [1]. Lattice mismatch with the sapphire is 18 % while that with the 6H-SiC is as little as 5 %.

In order to prepare epitaxial ZnO thin film on a transparent substrate, we attempted to grow ZnO (0001) on the (111) surface of YSZ (lattice mismatch: -10.5 %) utilizing the PLD method, and to study the electric properties of the resultant film.

4.2. Experimental

Oxygen gas was introduced into the chamber under pressure of 1.2 x 10^{-3} Pa. YSZ (111) and sapphire (0001) were used as a substrate. Substrate temperature was

maintained during film deposition at 600 °C or 800 °C. A ZnO ceramic target was set at the center of the PLD chamber, with the substrate positioned at the opposite side of the target. A ZnO film was deposited on the rotating substrate by focusing a KrF (λ=248 nm) excimer laser light onto the rotating target. The distance between the substrate and the target pellet was 30 mm. A pulsed laser with a repetition rate of 10 Hz was used; energy density was about 1～4 J/cm^2 per pulse.

Reflected high energy electron diffraction (RHEED) was used to monitor surface crystallinity. Film thickness was determined by use of a conventional stylus profilometer (Taylor-Hobson, Tallystep). An atomic force microscope (AFM, S.I.I., SPI-3700) was used to observe the film's surface morphology. The epitaxial relationship between the ZnO and substrate was studied by high-resolution XRD (Rigaku Co., ATX-G and ATX-E) measurements. Out-of-plane rocking curve measurement (ω scan) was performed as 2θ axis was fixed at ZnO (0002) diffraction angle. In-plane measurements were performed around critical angle of the X-ray total external reflection. The grazing incident angle of the X-ray was 0.3 °. In-plane rocking curve (ϕ scan) was measured as $2\theta\chi$ axis was fixed at ZnO (1100) diffraction angle. Cross-sectional views of the film were observed by a transmission electron microscope (TEM, JEOL, JEM 2000EX), and its electrical properties were measured at room temperature by the van der Pauw method.

4.3. Results

Polished YSZ substrates were annealed at 1350 °C for 1 h in air. Figure 4-1 shows an AFM image of the surface of YSZ (111) after the treatment. Flat terraces and step structures could be clearly observed. Terrace width was about 200 nm, and step

increments were about 0.3 nm which was in good agreement with the distance between two (111) planes of YSZ (0.297 nm). Flat terraces and step structures were also observed with the sapphire substrate annealed at 1500 °C for 1h in air.

Fifty-nm-thick ZnO films were grown on the annealed substrates of YSZ and sapphire surface by PLD at substrate temperatures of 600 °C. θ-2θ XRD patterns of the films showed only (0002) diffraction line of ZnO together with the substrate lines, indicating that c-axis of ZnO thin films oriented perpendicular to the substrate. Figure 4-2 shows the ZnO (0002) out-of-plane rocking curve of the ZnO / YSZ and the ZnO / sapphire. Full width at half maximum (FWHM) values for the ZnO / YSZ and the ZnO / sapphire were 0.12 ° and 1.7 °, respectively.

Figure 4-3 shows the cross sectional TEM images of the ZnO/YSZ and the ZnO/sapphire. Columnar structures 10nm wide and oriented perpendicular to the substrate surface are seen in ZnO/sapphire. Clear contrast is visible between individual columns, indicating that each columnar structure has a different crystal axis orientation. Columnar structures were also observed in ZnO/YSZ; here, width was about 50 - 100 nm and contrast was less clear.

The electric properties of the ZnO films are shown in Table 4-I. Hall mobility values for the ZnO / YSZ and the ZnO / sapphire were 45 cm^2/Vs and 7 cm^2/Vs, respectively.

Orientation of the ZnO thin films deposited on YSZ (111) surface at 800 °C was examined. RHEED patterns obtained at $[1\bar{1}00]$ and $[11\bar{2}0]$ of incident azimuth took on streak form. Figure 4-4(a) shows that FWHM of the ZnO (0002) rocking curve was 0.048° (173 arcsec). Figure 4-4(b) shows the XRD pattern of in-plane radial scan. This indicates that crystal orientation relationship was determined to be ZnO $(11\bar{2}0)$ // YSZ

$(1\bar{1}0)$.

Figure 4-5 shows an AFM image of the ZnO / YSZ (111) surface. Hexagonally shaped ZnO crystals were clearly observed. Film thickness was 150 nm. Terrace and step structures were observed in individual ZnO grains, with step heights between terraces of about 0.5 nm, indicating good agreement with the c-axis lattice constant of ZnO (0.52 nm). The relationship between ZnO grain size and film thickness is shown in Fig. 4-6. The grain size increased with film thickness.

Figure 4-7 shows changes in the Hall mobility and carrier density of ZnO / YSZ measured at 25°C, as a function of film thickness. Hall mobility rose toward 75cm^2/Vs as film thickness increased from 10 nm to 800 nm, while carrier density decreased.

4.4. Conclusions

Heteroepitaxial films of ZnO were grown on the (111) surface of YSZ and sapphire (0001) by the PLD method, using KrF eximer laser (λ=248nm) in an ultra-high-vacuum chamber at 600 °C. The epitaxial relationship between the ZnO / YSZ interface is ZnO $(11\bar{2}0)$ // YSZ $(1\bar{1}0)$. FWHM of the ZnO (0002) rocking curve of the ZnO / YSZ and ZnO / sapphire were 0.12 ° and 1.7 °, respectively. Cross-sectional TEM images suggested that ZnO on sapphire produced relatively larger amounts of twisted columns as compared to ZnO on YSZ. The Hall mobility of ZnO / sapphire was 7 cm^2/Vs, which was less than that of ZnO / YSZ (45 cm^2/Vs). Judging from these results, conduction carrier would be scattered at the boundaries of the twisted columns. The surface of heteroepitaxial ZnO film deposited at 800 °C was composed of hexagonally shaped grains. Flat terraces and step structures were observed in individual ZnO grains, and the step height between terraces was about 0.5 nm, which was in good agreement

with the lattice constant of c-axis of ZnO (0.52 nm). The grain size of ZnO increased with film thickness, while Hall mobility of ZnO / YSZ increased from 10 cm^2/Vs to 75 cm^2/Vs.

Acknowledgements

I would like to thank Dr. Katsuhiko Inaba and Mr. Isao Hamanaka of Rigaku Corporation for high-resolution XRD measurements.

References

[1] M. A. L. Jonson, S. Fujita, W. H. Rowland, Jr., W. C. Hughes, J. W. Cook, J. R. and J. F. Schetzina, *J. Electronic Materials* **25**, 855 (1996).

Table 4-I Electric properties of the ZnO deposited at substrate temperature of 600 °C.

Substrate	Electrical conductivity (S/cm)	Carrier density (/cm^3)	Hall mobility (cm^2/Vs)
YSZ (111)	8.7	1.2x10^{18}	45
Sapphire (0001)	7.3	6.6x10^{18}	6.9

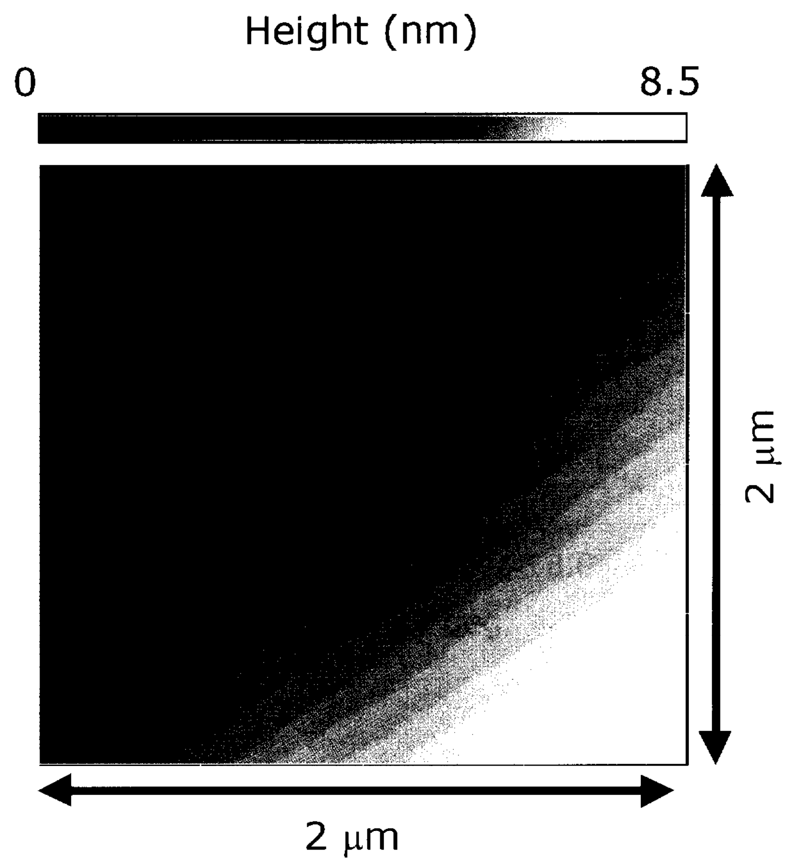

Figure 4-1 AFM image of surface of the YSZ (111) substrate annealed at 1350 °C for 1h in air.

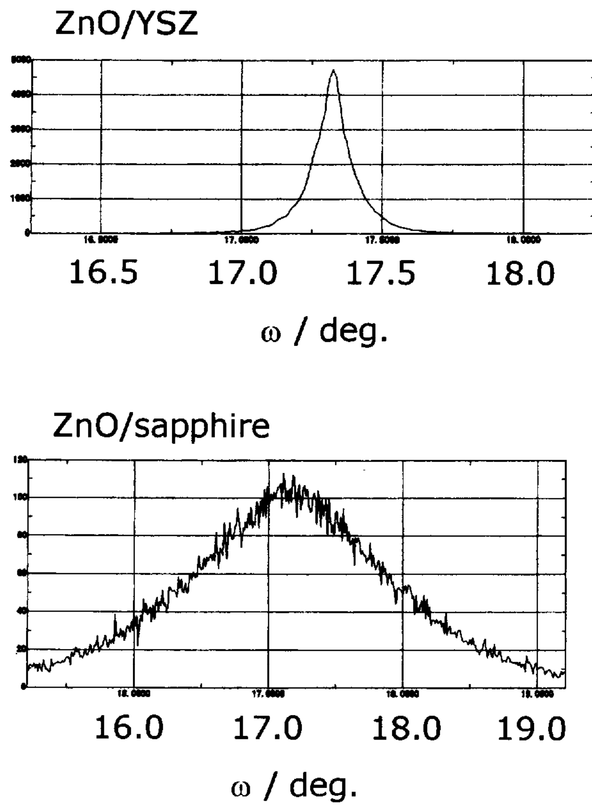

Figure 4-2 Out-of-plane rocking curve of ZnO (0002) deposited at substrate temperature of 600 °C.

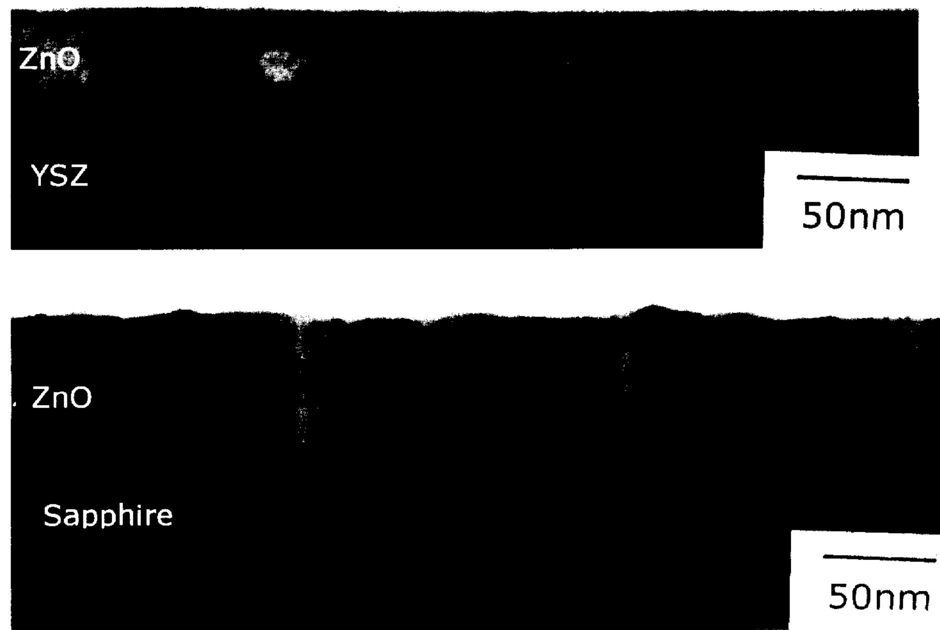

Figure 4-3 The cross-sectional bright field TEM images of ZnO/substrate.

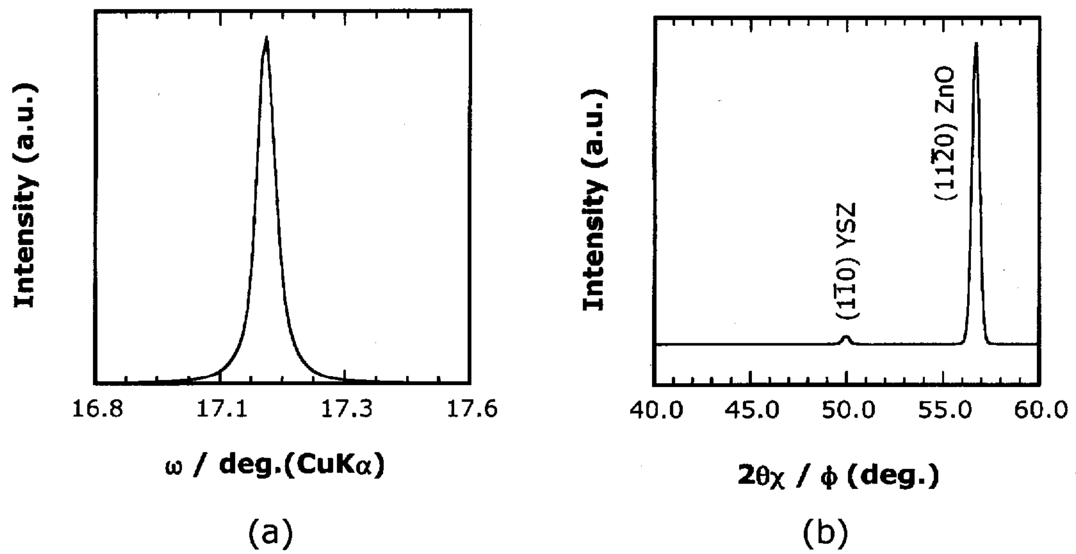

Figure 4-4 The high resolution XRD patterns of ZnO/YSZ deposited at substrate temperature of 800°C. (a) Out-of-plane rocking curve of ZnO (0002) and (b) in-plane diffraction pattern of 2θχ/φ radial scan (incident angle=0.3°, 2θ=31.75°)

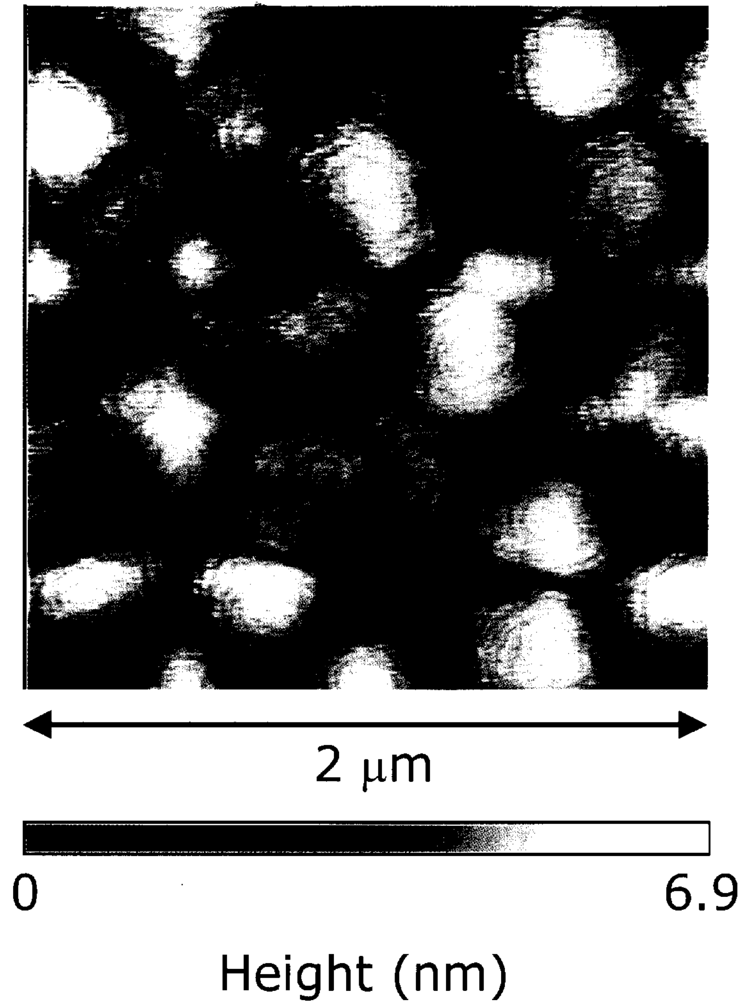

Figure 4-5 AFM image of the ZnO/YSZ deposited at the substrate temperature of 800°C.

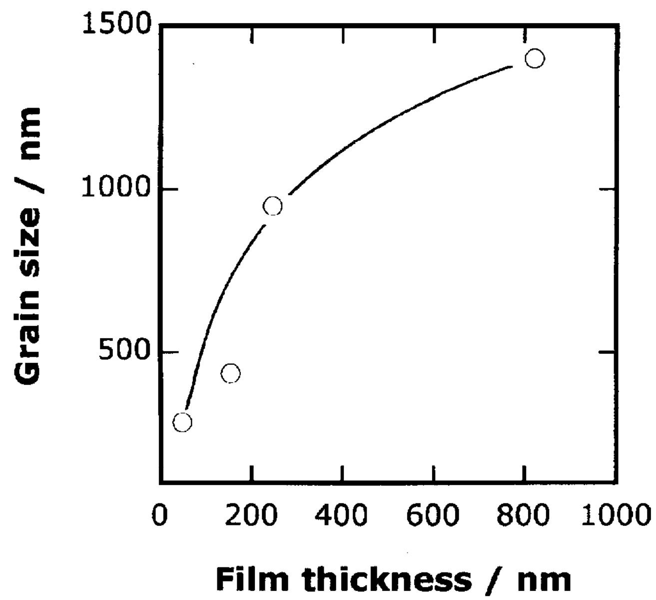

Figure 4-6 Relationship between the grain size of the ZnO estimated from AFM images and film thickness.

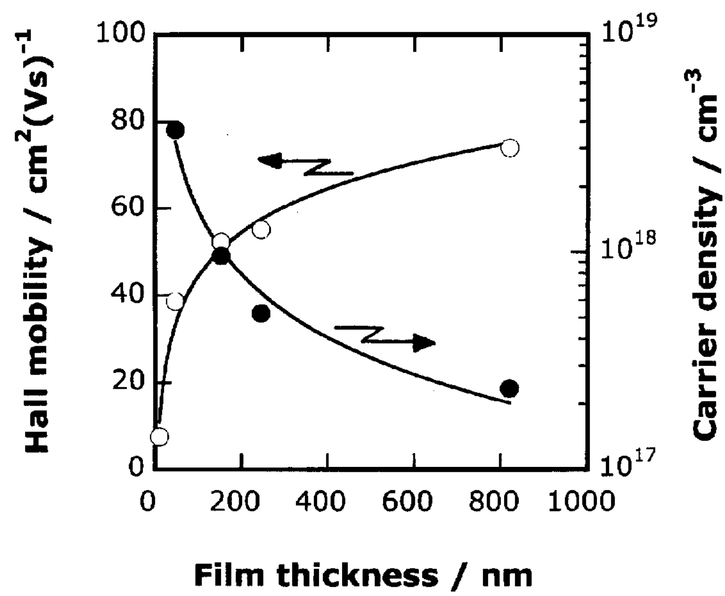

Figure 4-7 Changes in the Hall mobility and carrier density of ZnO/YSZ as a function of the film thickness.

Chapter 5. Electronic Structure and Optical Properties of P-type Transparent Oxide Semiconductor; $SrCu_2O_2$

5.1. Introduction

Interest in p-type transparent oxide semiconductors (TOSs) has rapidly grown in recent times, due primarily to strong demand for bipolar optoelectronic devices such as light-emitting diodes (LEDs), laser diodes (LDs), and solar cells. Although many n-type TOSs are already known, wide gap oxides exhibiting p-type conductivity remain rare.

Previously, we had developed several p-type TOSs, including $CuAlO_2$ [1], $CuGaO_2$ [2] and $CuInO_2$ [3] delafossites, and $SrCu_2O_2$ (SCO) [4], all containing Cu^+ as a major cationic species, according to the guidelines [1] for chemical modulation (d levels of Cu^+ primarily form the valence-band edge of the material) of the valence band. Further, several groups have recently reported p-type TOS with delafossite structure, which also contains Cu^+ as a major cationic species [5-7]. Electronic structure of $CuAlO_2$ delafossite has been clarified by photoelectron spectroscopy and band calculation [8], and compared with that of Cu_2O [9].

Among these p-TOSs materials, SCO is one of the most promising candidates for use in optoelectronic devices, mainly because the epitaxial films are obtained at relatively low temperature (350 °C), to prevent interface reactions at the junction region. We recently fabricated a UV-LED consisting of a p-n heterojunction, p-SCO and n-ZnO, which emits UV-light (λ = 382 nm) at room temperature [10], clear demonstration of SCO's suitability as an optically active p-TOS material for optoelectronic devices.

In this study, we examined through experiments the electronic structure of sintered bodies and thin films of SCO via photoelectron and optical spectroscopy. The

results are discussed by comparing calculated energy band structures in order to clarify the origin of p-type conduction in SCO.

5.2. Experimental

5.2.1. Energy Band Calculation

Figure 5-1 shows the crystal structure of SCO, which belongs to the $I4_1/a\ m\ d$ space group [11]. The cell parameters are a = b = 0.5469 nm and c = 0.9826 nm. The zigzag chains of the O-Cu-O dumbbells are observed to align along the a- and b-axis directions ([100]). Energy band calculations for the crystal structure were performed by the first-principle plane-wave pseudopotential method (Cambridge Sequential Total Energy Package, CASTEP [12]) under local density approximation (LDA). The total density of states (DOS) and partial density of states (PDOS) were also calculated by this method.

5.2.2. Bulk Ceramic Preparation and PES / IPES Measurement

A sintered specimen of K^+-doped SCO ($Sr_{0.95}K_{0.05}Cu_2O_2$) was fabricated by a conventional ceramic process. Stoichiometric mixtures of Cu_2O, $SrCO_3$, and K_2CO_3 powders were calcined at 950 °C for 40 h in an N_2 atmosphere, after which the calcined powder was reground and pressed into a disk. Subsequently, the disk was sintered at 850 °C for 10 h in an N_2 atmosphere. The specimen was identified by the powder X-ray diffraction method as a single phase of the $SrCu_2O_2$ crystal. The positive hole concentration of the specimen estimated by Hall measurement was approximately 10^{18} cm^{-3}.

Photoemission spectroscopy (PES) / Inverse Photoemission Spectroscopy (IPES)

measurements were performed at room temperature on the sintered specimen, using an instrument built in our laboratory composed of an ultra high vacuum chamber, a hemisphere-shaped analyzer, and both ultraviolet light (He I, II) and X-ray (Mg Kα) sources. The clean surface was obtained by scraping the specimen with a diamond file under ultra-high vacuum before measurement. PES and IPES measurements were completed under an ultra-high vacuum of 4∼5 x 10^{-7} Pa and 5∼6 x 10^{-8} Pa, within 30 min and 60 min, respectively, to avoid surface contamination of the specimen. For the ultraviolet photoelectron spectroscopy (UPS) measurement, UV light of He I resonance radiation, 21.2 eV, was used for excitation, while Mg Kα X-ray (1254 eV) was used in the X-ray photoelectron spectroscopy (XPS). The IPES spectrum was measured in bremsstrahlung isochromat spectroscopy (BIS) mode by monitoring the intensity of 9.4 eV photons emitted from the sample. The resolutions of PES and IPES measurements were ∼100 meV and ∼500 meV, respectively. The origin of the binding energy scale was set to the Fermi level, which was determined by referring to the Fermi level of Au sputtered onto the specimen. The UPS and IPES spectra for each specimen were connected at the Fermi level.

5.2.3. Thin Film Preparation and Optical Measurement

SCO thin film was grown heteroepitaxially on a YSZ (111) surface by the pulsed-laser deposition (PLD) method at a substrate temperature of 800 °C. The resulting thin film was shown by high resolution X-ray diffraction analysis to be highly (112) oriented SCO crystal.

The optical properties of the SCO film were measured at 7 – 300 K using a conventional spectrophotometer and a cryostat. Photoluminescence (PL) spectra were

taken with a monochromator equipped with a time-gated multi-channel detector, in which a 4ω-YAG laser (266 nm) was employed as the excitation light source. The excitation spectrum for the blue-green emission band (PLE) was measured using monochromatized light from an Xe-lamp as an excitation light source.

5.3. Results and Discussion

5.3.1. Energy Band Diagram

Figure 5-2 shows the calculated energy band structure of SCO along the symmetry lines in the Brillouin zone. Both the bottom edge of the conduction band and the upper edge of the valence band are located at Γ point, indicating a direct-type band gap. In the top of the valence band, the curvature in Γ-X ([100]) or Γ-M ([110]) is greater than in the Γ-Z ([001]) direction. Since the curvature of the band is inversely proportional to the effective mass, the zigzag chain of O-Cu-O dumbbells directing [100] and [010] axis is likely responsible for positive hole transport in SCO.

Figure 5-3 shows the calculated total DOS and PDOS of SCO. The energy states around the conduction and valence band edges are mostly composed of the 3d, 4p, and 4s electrons of Cu^+, and the 2p of O^{2-}, while the orbitals of Sr^{2+} ions contribute slightly. The valence band maximum is dominantly composed of Cu d, Cu s, and O p states and four distinct bands are additionally observed in the valence band. On the other hand, Cu p-, Cu s- and O p-states mostly constitute the conduction band minimum, and a sizable contribution of Cu d-states to the valence band is observed.

Electronic structure of Cu_2O, known as a p-type semiconductor, has been investigated intensively, in which a good agreement of calculated DOS spectra [13] with experimental results including X-ray absorption spectra [14-15], has been obtained. As

schematically shown in Fig. 5-4, a sizable covalent contribution of Cu – O bonds in this compound induces the mixture of Cu 3d with Cu 4sp orbital. The resultant mixed orbital is split into states labeled by the irreducible representation of the point symmetry group for Cu site due to the crystal ligand field. Those states further interact with crystal field split states originated from ligand oxygen 2p orbital, when the both states belong to the same irreducible representation. Some of the split states may remain non-interacted or slightly interacted due to lack of counterpart states having the same irreducible representation. Those are tentatively named "non-bonding state", while the interacted states result in forming a combination of "bonding state" and "anti-bonding state". The anti-bonding state, the mixture of Cu 3d and 4sp with O 2p, constitutes the valence band maximum. On the other hand, the conduction band is primarily composed of Cu 4sp and O 2p with slight contribution of Cu 3d. Thus, it appears that the band edge transition involves partly the intra-atomic transition of Cu^+.

The compositional similarity between Cu_2O and SCO, together with the fact that the DOS spectra of Cu_2O is in reasonably good agreement with that of SCO in Fig. 5-3, suggests that the basic electronic structure of SCO around the energy gap region is quite similar to that of Cu_2O, except a considerably larger energy gap of SCO (~3.3 eV) compared with that of Cu_2O (2.17 eV). Thus, by comparing the empirical energy diagram in Fig. 5-4 with DOS spectrum in Fig. 5-3, it is concluded that band I, located at the valence band maximum, is assigned as "anti-bonding state of Cu 3d and 4sp with O 2p", while bands II, III, and IV are to "non-bonding state of Cu 3d and 4p", "non-bonding state of O2p", and "bonding state of Cu3d and 4sp with O 2p", respectively.

5.3.2. PES/IPES Measurement

UPS, XPS and IPES spectra of the K^+-doped SCO are shown in Fig. 5-5. The Fermi energy lies around the edge of the valence band, demonstrating that the sample exhibits p-type conductivity. The band gap, observed between the top of the valence band and the bottom of the conduction band in the PES / IPES spectra, was estimated to be ~ 3 eV, in reasonable agreement with the band gap evaluated by optical measurement (~ 3.3 eV) [4]. Two bands indexed as A (~ 3 eV in the XPS spectrum) and B (~ 6 eV in the UPS spectrum) were observed in the PES spectra, while the IPES was featureless. The intensity of band A is enhanced in the XPS spectrum, while band B is enhanced in the UPS spectrum. This observation and the binding energy of each band indicate that the original states of band A and B are associated with Band II and Band III, respectively, since the d-state has a larger ionization cross-section for higher energy photons compared to the p-state [16].

5.3.3. Optical Properties

Figure 5-6 shows the optical absorption (α) and photoluminescence (PL) spectra of the SCO film measured at 7 K. A sharp absorption band peaking at 3.46 eV (band A) is observed. Located near the fundamental absorption edge, band A has a relatively large absorption coefficient of 1.5 x 10^5 cm^{-1}, with a narrow bandwidth, indicating that the absorption peak originates from the exciton at the Γ point. Since both the valence and conduction band edges at the Γ point were split into multi-valleys as a result of tetragonal crystal field and spin orbit interaction, the valley with which the exciton is associated is uncertain. Photoluminescence peaking near the absorption edge was not detected, but an intense blue-green emission band centering at 2.47 eV (band B) was observed. The excitation spectrum for the emission, also shown in the figure, indicates

that the emission was induced efficiently through excitonic absorption (band A), but not so efficiently by absorption at higher energy to the conduction band continuum.

The time-resolved emission spectra for band B at 7 K (Fig. 5-7) reveals that the band shape, including peak position, remained unchanged with time delay. The peak position did not shift due to the change in the excitation intensity. These observations rule out the possibility that the emission results from donor-acceptor pair recombination. (If this were the case, a spectral red shift would be observed, with an increase in delay time and a decrease in excitation intensity.) The emission lifetime obtained from the spectra is 17.8 μsec, which implies that the transition responsible for the emission has partially allowed nature. It has been reported that similar emissions observed in Cu^+ doped materials such as $CuLaO_2$ are assigned as a Cu^+ 4s→3d transition [17]. These facts suggest that the observed emission band is attributable to Cu^+ intra-atomic transitions partially allowed through the mixing of p orbital of both Cu and O into 3d and 4s states.

5.4. Conclusions

The electronic structure of a wide band gap (~3.3 eV) p-type oxide semiconductor, $SrCu_2O_2$, is examined via photoelectron and optical spectroscopy, and the experimental results are compared with the calculated energy band structure by the local density approximation method. The main results are summarized as follows:

(1) Fermi energy measured by PES / IPES lies around the edge of the valence band, evidence that $SrCu_2O_2$ is a p-type conductor.

(2) The valence band maximum is formed by the anti-bonding state of Cu 3d and

4sp with O 2p, while the conduction band minimum is primarily composed of Cu 4sp and O 2p, forming a direct energy band gap at the Γ point.

(3) Large dispersion of the valence band maximum along [100] and [010] directions, likely related to the zigzag chain of O-Cu-O dumbbell structure, is responsible for the positive hole conduction path.

(4) A sharp absorption band observed at the fundamental absorption edge was tentatively attributed to exciton. Instead of a corresponding emission band without a Stokes shift, a blue-green emission band peaking at ~2.47 eV (Stokes shift of ~1 eV) was observed, likely associated with the intra-atomic transition of Cu^+, that is partially allowed by mixing of p-orbital.

References

[1] H. Kawazoe, M. Yasukawa, H. Hyodo, M. Kurita, H. Yanagi and H. Hosono, *Nature (London)* **389**, 939 (1997).

[2] H. Yanagi, H. Kawazoe, A. Kudo, M. Yasukawa and H. Hosono, *J. Electroceram.* **4**, 427 (2000).

[3] H. Yanagi, T. Hase, S. Ibuki, K. Ueda and H. Hosono, *Appl. Phys. Lett.* **78**, 1583 (2001).

[4] A. Kudo, H. Yanagi, H. Hosono and H. Kawazoe, *Appl. Phys. Lett.* **73**, 220 (1998).

[5] R. E. Stauber, J. D. Perkins, P. A. Parilla and D. S. Ginley, *Electrochem. Solid-State Lett.* **2**, 654 (1999).

[6] H. Gong, Y. Wang and Y. Luo, *Appl. Phys. Lett.* **76**, 3959 (2000).

[7] N. Duan, A. W. Sleight, M. K. Jayaraj and J. Tate, *Appl. Phys. Lett.* 77, 1325 (2000).

[8] H. Yanagi, S. Inoue, K. Ueda, H. Kawazoe, H. Hosono and N. Hamada, *J. Appl. Phys.* **88**, 4159 (2000).

[9] A. Buljan, M. Llunell, E. Ruiz and P. Alemany, *Chem. Mater.* **13**, 338 (2001).

[10] H. Ohta, K. Kawamura, M. Orita, M. Hirano, N. Sarukura and H. Hosono, *Appl. Phys. Lett.* 77, 475 (2000).

[11] L. Teske and Hk. Muller-Buschbaum, *Z. Anorg. Allg. Chemie.* **379**, 113 (1970).

[12] M. C. Payne, M. P. Teter, D. C. Alan, T. A. Arias and J. D. Joannopoulos, *Rev. Mod. Phys.* **64**, 1045 (1992).

[13] L. Kleinman and K. Mednick, *Phys. Rev.* **B 21**, 1549 (1980).

[14] M. Grioni, J. F. van Acker, M. T. Czyzyk and J. C. Fuggle, *Phys. Rev.* **B 45**, 3309 (1992).

[15] T. S. Niedrig, T. Neisus, I. Bottger, E. Kitzelmann, G. Weinberg, D. Demuth and R.

Schlogl, *Phys. Chem. Chem. Phys.* **2**, 2407 (2000).

[16] Atomic Calculation of Photoionization Cross-Sections and Asymmetry Parameters edited by J. –J. Yen (Gordon and Breach, Pennsylvania, 1993).

[17] C. Parent, P. Boutinaud, G. L. Flem, B. Moine, C. Pedrini, D. Garcia and M. Faucher, *Opt. Mater.* **4**, 107 (1994).

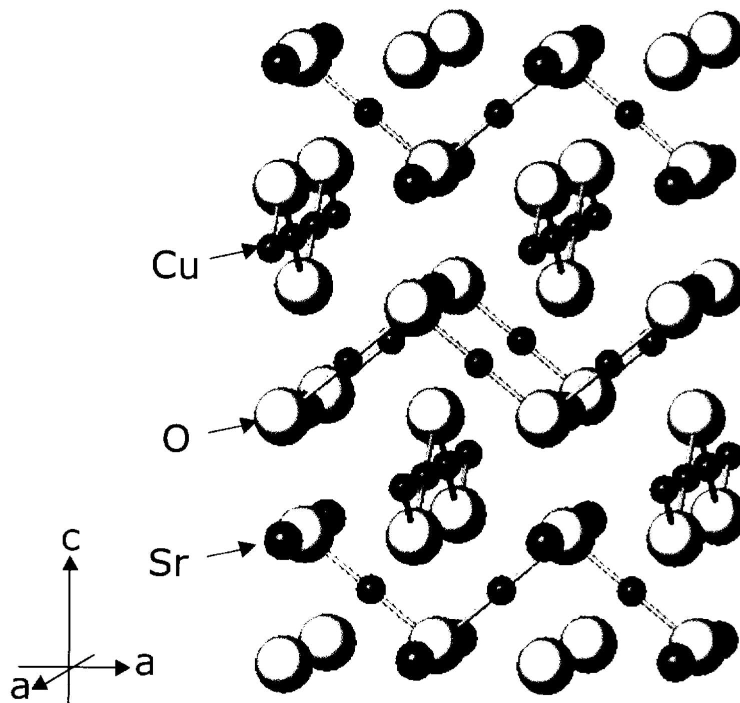

Figure 5-1. Schematic illustration of crystal structure of $SrCu_2O_2$. Zigzag chains of O-Cu-O dumbbell-shaped structure are aligned [100] and [010] directions.

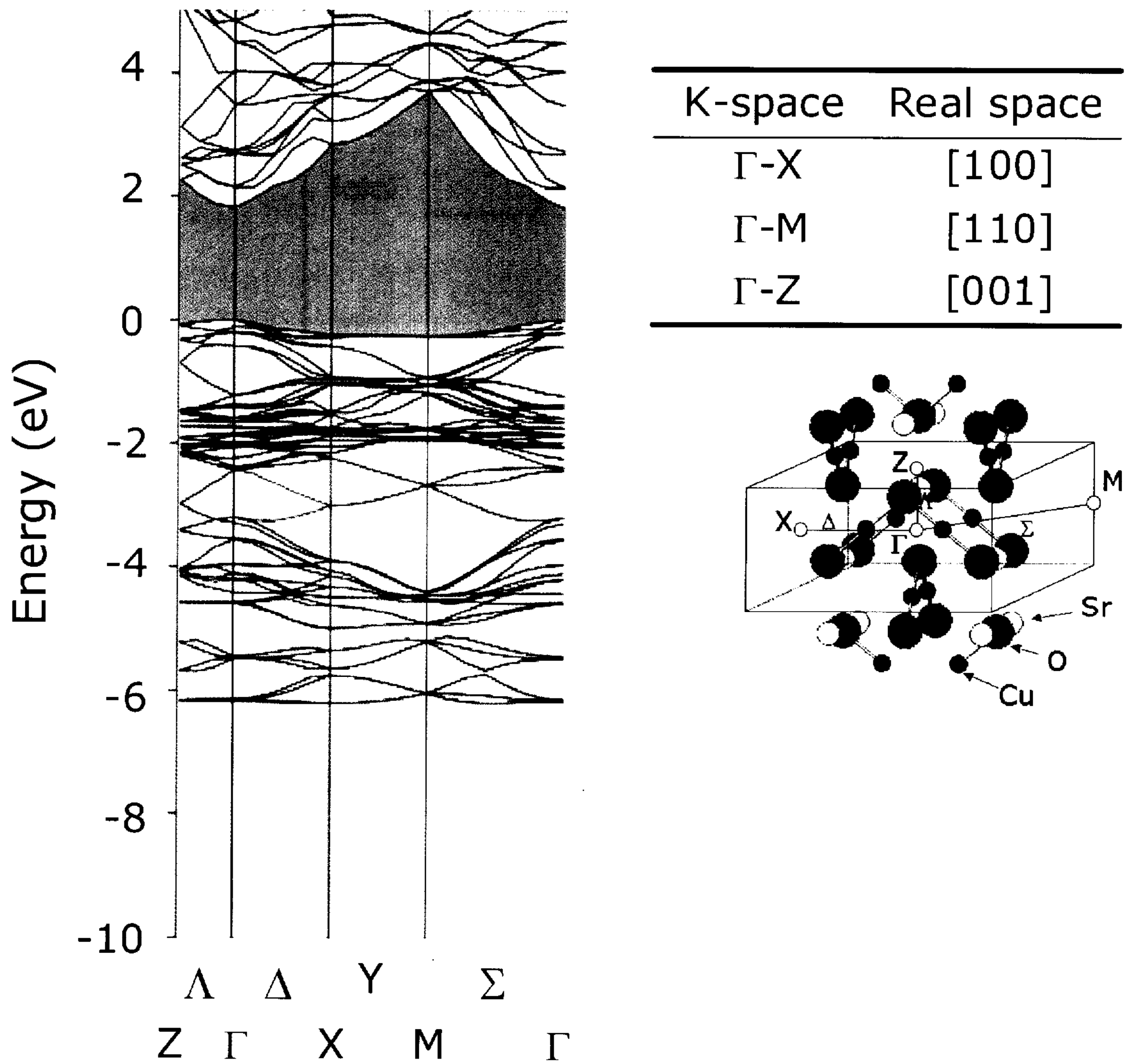

Figure 5-2. The calculated energy band structure of $SrCu_2O_2$ along the symmetry lines in the Brillouin zone. The dispersion of Γ-X ([100]) or Γ-M ([110]) is larger than that of Γ-Z ([001]) direction.

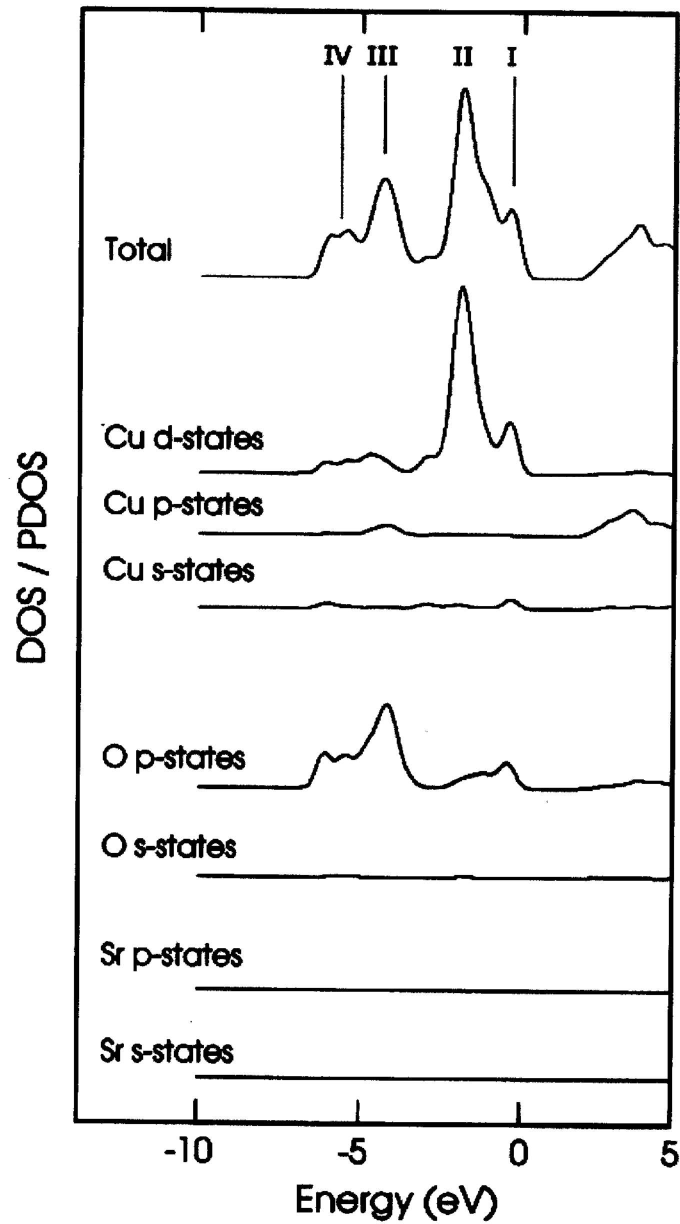

Figure 5-3. The calculated total DOS and PDOS of $SrCu_2O_2$. The valence band maximum is formed by the anti-bonding state of Cu 3d and 4sp with O 2p, while the conduction band minimum is primarily composed of Cu 4sp and O 2p.

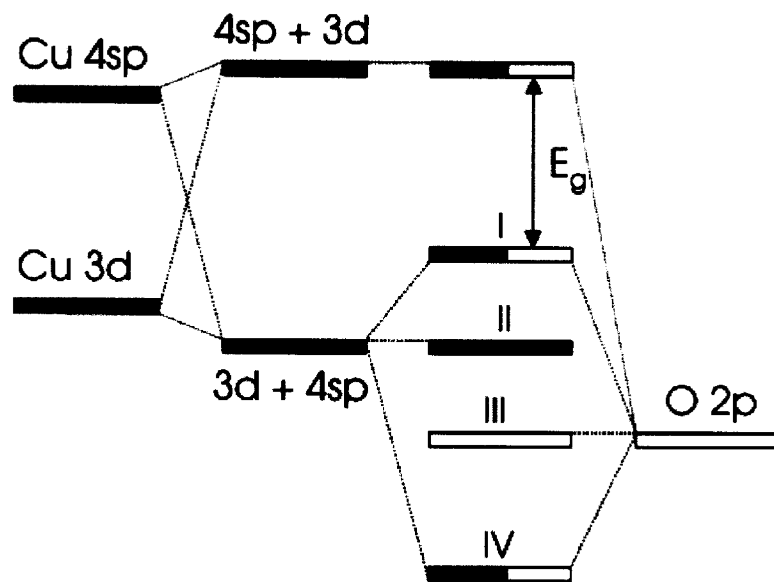

Figure 5-4. Schematic illustration of the electronic structure of Cu_2O, basically applicable to that of SCO. Band I, II, III and IV are tentatively named as "Anti-bonding state of Cu and O", "Non-bonding state of Cu", "Non-bonding state of Cu", "Non-bonding state of O" and "Bonding state of Cu and O".

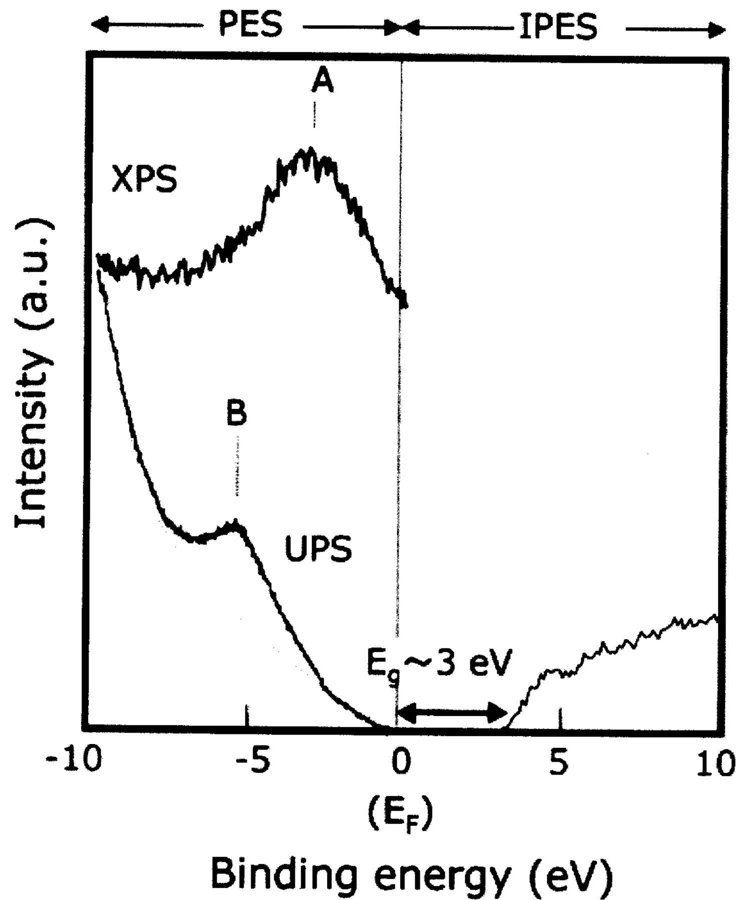

Figure 5-5. PES (XPS and UPS) and IPES spectra of K^+-doped $SrCu_2O_2$. K^+ ion was doped to enhance the electrical conductivity. No significant change in the spectral shape was observed by the doping. Monotonic increase in background intensity in UPS is due to the inelastic electron scattering. Fermi energy level is located near the upper edge of valence band maximum, demonstrating p-type conductor. Band A in XPS and Band B in UPS are attributed to Band II and III in Fig. 5-4.

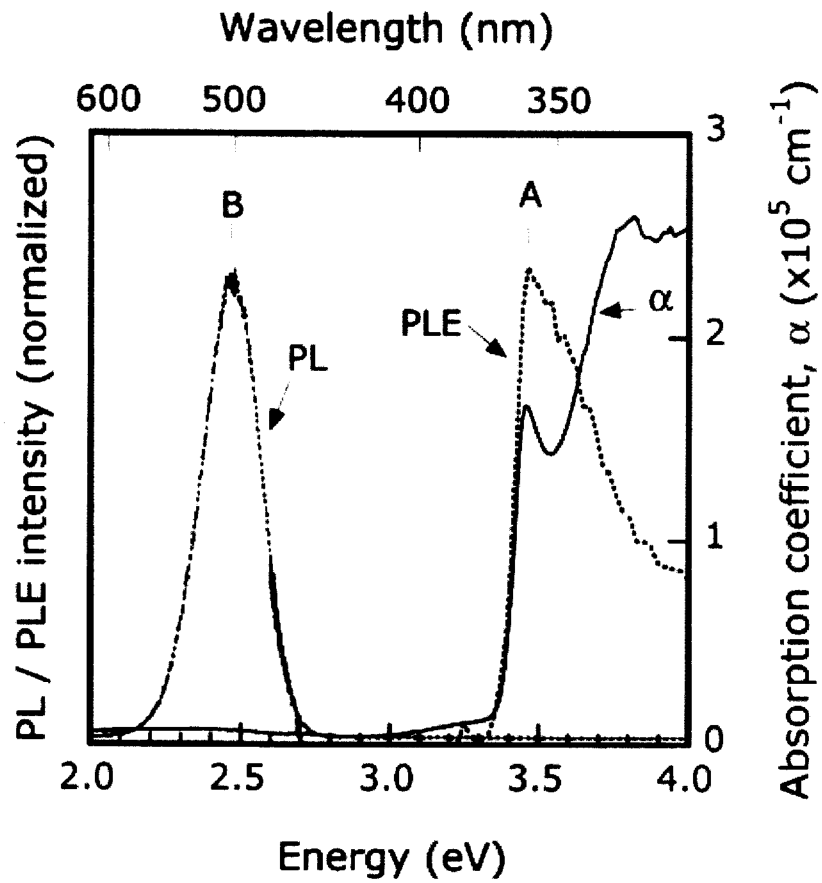

Figure 5-6. Photoluminescence (PL) and absorption (α) spectra of $SrCu_2O_2$ thin film measured at 7 K. Excitation spectrum (PLE) for emission band B is also shown.

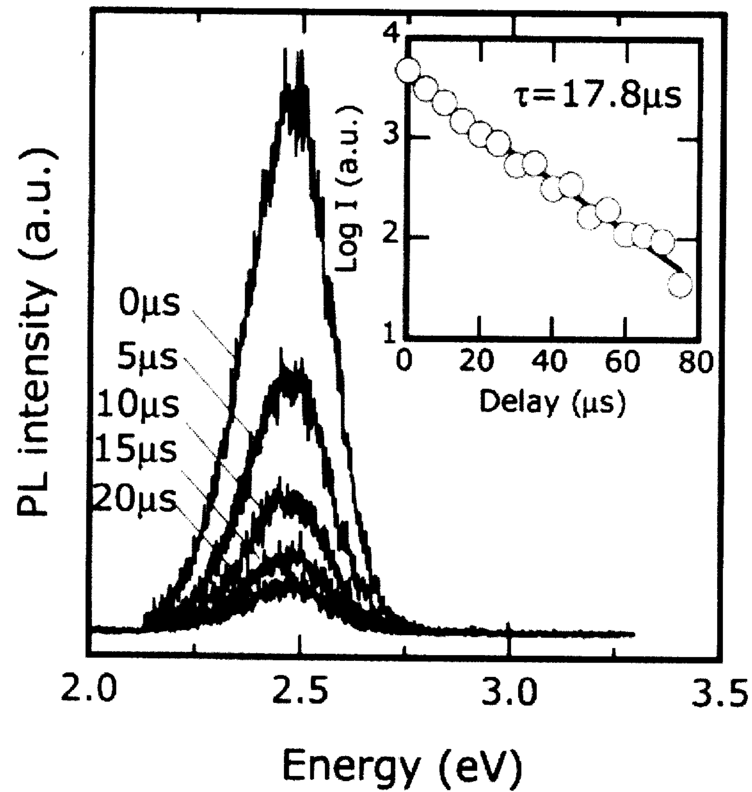

Figure 5-7. Time resolved photoluminescence spectra of $SrCu_2O_2$ thin film at 7 K. The inset shows a semi-log plot of the emission intensity (I) with decay time (t). The emission lifetime (τ) is obtained as 17.8 μsec using $I = I_0 \exp(-t / \tau)$.

Chapter 6.
Fabrication and Characterization of Ultraviolet-Emitting Diodes Composed of Transparent P-N Heterojunction, p-$SrCu_2O_2$ and n-ZnO

6.1. Introduction

Transparent oxide semiconductors (TOSs) have yet to be incorporated into opto-electronic devices, in particular into light-emitting diodes (LEDs) and laser diodes (LDs), due to the lack of TOSs that exhibit p-type conductivity. For example, ZnO has been known to emit visible light efficiently when excited with either electron beams or UV light. The combination of this feature together with n-type conductivity has been commercialized as green phosphor for vacuum fluorescence devices and CRTs. The material is also promising for potential use as a UV light-emitting phosphor (emission wavelength~380 nm) at room temperature due to free excitons, having sufficiently large binding energy (60 meV) [1] to be stable even at room temperature. Laser operations excited with electron beams [2] or UV light [3-5] have been reported so far. UV-LEDs based on metal-insulator-semiconductor (MIS) junctions have been reported based on Ag/SiO/ZnO [6], Au/SiO/ZnO [7] and Cu_2O/ZnO [8]. However, no UV-emission based on p-n junctions has been realized to date, due to the difficulty of fabricating p-type ZnO, although several attempts including laser doping [9] or co-doping [10] have been made.

Our approach to realizing a ZnO-based p-n junction LED is unique in that it uses TOSs exhibiting p-type conductivity other than p-ZnO as a partner of n-ZnO to form the p-n heterojunction, rather than developing a p-n homojunction of ZnO. Among several p-type TOSs [11-13] that we have created to date, p-$SrCu_2O_2$ was selected for

this study, primary because it can be deposited at temperatures as low as 350 °C. The low temperature deposition process makes it possible to minimize chemical reaction at the $SrCu_2O_2$/ZnO interface. Additionally, $SrCu_2O_2$ can be hetero-epitaxially grown on (0001) plane of ZnO with hexagonal lattice, since Cu^+ or O^{2-} ions in both (112) and (100) planes of $SrCu_2O_2$ have six-fold symmetry. They may also be lattice-matched if so called domain matched epitaxy is taken into consideration. In general, epitaxial growth is to possibly result in the formation of high quality, optically active p-n junctions.

In the previous letter, we reported for the first time the formation of a p-n heterojunction composed of this combination that demonstrated typical electrical current-rectifying behavior and UV-light emission due to current injection [14]. This paper provides a detailed description of heteroepitaxy, which depends strongly on growth temperature and the improved optical characteristics of heterojunction diodes composed of p-$SrCu_2O_2$ and n-ZnO.

6.2. Experimental

Multi-layered films were grown by a pulsed-laser-deposition (PLD) technique. We have already described our PLD apparatus in previous papers [11-16]. A yttria-stabilized-zirconia (YSZ) single crystal (111) plate with an extremely flat surface was used as a substrate. Indium-Tin-Oxide (ITO), used as a transparent n-electrode, was grown at 900 °C on the substrate. Then n-ZnO and p-$SrCu_2O_2$ layers were successively deposited in the same PLD chamber. The deposition of ZnO on the ITO layer allows us to deposit ZnO layer at temperatures up to 800 °C, resulting in good crystal quality for ZnO films. $SrCu_2O_2$ was grown at substrate temperatures of 350 °C (film A) or 600 °C (film B and C; film C was obtained with the same condition as

sample B, except the higher laser irradiation energy density onto the target. The energy density of film C was 4 J/cm^2/pulse, while that of film A and B was 2.5 J/cm^2/pulse.) N-type ZnO conductivity was achieved by controlling the deposition atmosphere. K^+ ions were doped into Sr^{2+} sites in $SrCu_2O_2$ to control p-type conductivity. The carrier density of each layer was matched and set to 5 x 10^{17} cm^{-3}. Secondary ion mass spectrometry (SIMS) analysis was performed to check the diffusion of dopant ions across the junction. Finally, a nickel metal layer used as a p-electrode was deposited on top of the multi-layered film. The film thickness of ZnO and $SrCu_2O_2$ layers were set at 500 nm and 200 nm, respectively, which were thicker than the depletion layer (~100 nm) of the p-n heterojunction. The multi-layered film prepared by PLD was processed by conventional photo-lithography followed by a reactive ion etching process to fabricate a mesa structure having a surface area of 0.5 mm x 0.5 mm. Figure 6-1 is a schematic diagram of the LED device used in this study. The LEDs prepared using films A, B and C were named LED A, B and C, respectively, hereafter.

Crystalline quality and orientation were analyzed by high-resolution X-ray diffraction measurements (HR-XRD, ATX-G, Rigaku Co.). The out-of-plane reciprocal-space mapping (separate scan of 2θ and ω in the horizontal plane), in-plane reciprocal-space mapping (separate scan of $2\theta\chi$ and ϕ in the azimuth plane), out-of-plane rocking curve (2θ fixed ω scan) and in-plane rocking curve ($2\theta\chi$ fixed ϕ scan) were obtained. The lattice image near the $SrCu_2O_2$/ZnO interface was examined by high-resolution transmission electron microscopy (HR-TEM, JEM-2000EX, JEOL).

I-V characteristics were evaluated by applying DC voltage to the diode. The

electro-luminescence (EL) resulting from electric current injection or photo-luminescence (PL) excited with He-Cd (325 nm) laser irradiation was measured by introducing emission light into a bundle fiber through the transparent n-electrode (ITO), and guided to a spectrometer with a multi-channel detector.

6.3. Results and Discussion

6.3.1. Crystal Quality and Orientation of The Multilayered Films

Figure 6-2 shows out-of-plane reciprocal-space mappings of multi-layered films of film A (a) and film B (b). Film C exhibited mappings quite similar to that of film B. The figures indicate that the preferential orientation of $SrCu_2O_2$ on ZnO (0001) was $SrCu_2O_2$ (112)/ZnO (0001) at 350 °C, which was changed to $SrCu_2O_2$ (100)/ZnO (0001) at 600 °C. Further, it was noticed that full-width at half maximum (FWHM) of the out-of-plane rocking curve of $SrCu_2O_2$ improved from 1 to 0.3 degree with increasing deposition temperatures. The improved value was almost the same as that of ZnO (0.2 degree), indicating that the tilting angle of the $SrCu_2O_2$ crystal was reduced to the similar level of ZnO layer, due to the improved crystallinity of the $SrCu_2O_2$ layer deposited at higher temperatures.

Figure 6-3 shows in-plane reciprocal-space mappings of film A (a) and film B (b). Two distinct diffraction peaks of (022) and $(2\bar{2}0)$ from $SrCu_2O_2$ together with $(11\bar{2}0)$ ZnO were observed in Fig. 6-3(a), implying that two types of crystallographic domains are involved in the $SrCu_2O_2$ layer. On the other hand, observation of only the {011} diffraction peak of $SrCu_2O_2$ in Fig. 6-3(b) clearly demonstrates that $SrCu_2O_2$ layers deposited at 600 °C were grown heteroepitaxially on ZnO with single crystallographic domain.

Figure 6-4 shows a cross-sectional HR-TEM image near the p-n heterojunction region of film A (a) and film B (b), where the electron beams were injected along [11$\bar{2}$0] of ZnO. The stacking of ZnO (0001) and $SrCu_2O_2$ (112) planes in terms of deposition direction clearly appears as having a very abrupt hetero-epitaxial interface in Fig. 6-4(a). It also appears that the $SrCu_2O_2$ layer is composed of several crystallographic domains. Such spatial inhomogeneities were not seen in Fig. 6-4(b), but $SrCu_2O_2$ (200) planes were heteroepitaxially grown on ZnO (0001) plane. These observations are in good agreement with those by HR-XRD.

6.3.2. UV-Light Emission due to Hetero P-N Junction

Figure 6-5 shows the I-V characteristics of LED A and B when DC bias was applied to the electrode, which demonstrated rectifying behavior inherent to p-n heterojunctions. The I-V curves scattered considerably and the current started to flow with relatively low voltage in LED A. On the other hand, the I-V curve of LED B did not fluctuate largely and turn-on voltage was obtained approximately as 3 V, in good agreement with the energy band gap for ZnO (3.3 eV).

An UV emission band centered at 382 nm was obtained at room temperature when a forward bias voltage greater than 3 V was applied to the p-n heterojunction of LED B. Similar emission was also detected in LED A when the junction tolerated the application of the voltage larger than $\sim$2 V. For comparison, Fig. 6-6 also shows the photoluminescence (PL) excited by a 325 nm He-Cd laser light. The shift in emission bands between PL and EL observed in Fig. 6-6 is most likely due to differences in excited state density. The density in PL was estimated to be on the order of 10^{14} cm^{-3}, while the density in the case of EL was estimated to be approximately 10^{17} cm^{-3}. The PL

band is assigned as the free exciton decomposition in ZnO, while the EL is attributable either to the "P band," which is considered to be transition-associated with exciton-exciton collision, or to the "N band" assigned as electron-hole plasma recombination [5,17].

Fig. 6-7 shows the emission spectra for several injection electric currents. Increased EL intensity with an increase in injection current was noticed without significant change in band shape or peak energy. The threshold currents of UV emission for LED A and B were 10 mA and 2 mA, respectively.

Figure 6-8 shows EL intensity as a function of the forward bias voltage applied to the diode for LED B. The turn-on voltage was about 3 V, in good agreement with the energy difference between the ZnO donor level and the $SrCu_2O_2$ acceptor level, as illustrated in Fig. 6-9. The agreement provides clear evidence that the EL band arises due to electric current injection through the p-n heterojunction. In the case of LED A, a difference in turn-on voltage between EL intensity-V and I-V characteristics was observed, which may be attributed to spatial inhomogeneities in the interface, as suggested by the HR-XRD and the cross-sectional HR-TEM image. That is, an optically inactive p-n heterojunction was partially formed, whose turn-on voltage in the I-V curve was likely lower than one that was intrinsic. In contrast, in the case of LED B, the turn-on voltages of both EL intensity-V and I-V characteristics agree quite well.

These observations indicate that improved performance of the p-n heterojunction was obtained for higher deposition $SrCu_2O_2$ temperatures, accompanied by enhanced LED efficiency by an order of magnitude of up to 0.01 %.

6.3.3. Visible Light Emission due to Hetero P-I-N Junction

Figure 6-10 shows an I-V characteristic of a fabricated diode using film C. No current was observed for a bias voltage less than 14 V applied both in the forward and reverse directions. Electric current increased suddenly when bias voltages exceeded 14 V, a value considerably greater than the intrinsic energy gap of either ZnO or $SrCu_2O_2$. Such behavior is common to the semiconductor/insulator interface. SIMS analysis revealed that K^+ ions had diffused noticeably into the ZnO layer. The $SrCu_2O_2$ layer in film C was deposited with intense irradiation energy density at 600 °C relative to film B, which may enhance the diffusion of K^+. Thus, it was thought that the p-i-n heterojunction was formed in film C due to charge compensation between the donor (interstitial Zn atom and/or oxygen vacancy) and the acceptor (K^+ ion).

Figure 6-11 shows the electro-luminescence spectrum of the diode. Visible broadband emission centered at 500 nm was observed instead of the UV band by applying a forward bias voltage larger than 14 V, where a hole or electric current was injected into ZnO or $SrCu_2O_2$ layer.

6.4. Conclusions

A UV light-emitting diode was fabricated using a hetero p-n junction composed of the transparent conductive oxides p-$SrCu_2O_2$ and n-ZnO. The out-of-plane preferential orientation of $SrCu_2O_2$ on ZnO (0001) was changed from $SrCu_2O_2$ (112)/ZnO (0001) to $SrCu_2O_2$ (100)/ZnO (0001) with an increase in the growth temperature of $SrCu_2O_2$. The device fabricated from the film at the higher growth temperature exhibited rectifying I-V characteristics inherent in p-n junctions whose turn-on voltage is about 3 V. A relatively sharp electro-luminescence band centered at 382 nm was generated by

the application of a forward bias voltage larger than the turn-on voltage of 3 V, which is in agreement with the theoretical value. UV-LED characteristics such as threshold current of UV emission (from 10 to 2 mA) and emission efficiency (up to 0.01 %) were improved by increasing $SrCu_2O_2$ deposition temperatures from 350 to 600 °C. When the laser irradiation energy density was increased at 600 °C, the incidence of insulator layer formation due to the diffusion of K^+ ions into ZnO increased. The resulting p-i-n diode emits a visible electro-luminescence band centered at 500nm when a bias voltage greater than 14 V is applied.

Acknowledgement

The authors would like to thank Mr. S. Takeda of Asahi Glass Company for SIMS measurement.

References

[1] D. G. Thomas, *J. Phys. Chem. Solids* **15**, 86 (1960).

[2] F. H. Nicoll, *Appl. Phys. Lett.* **9**, 13 (1966).

[3] D. C. Reynolds, D. C. Look and B. Jogai, *Solid State Commun.* **99**, 873 (1996).

[4] D. M. Bagnall, Y. F. Chen, T. Yao, S. Koyama, M. Y. Shen and T. Goto, *Appl. Phys. Lett.* **70**, 2230 (1997).

[5] P. Zu, Z. K. Tang, G. K. L. Wong, M. Kawasaki, A. Ohtomo, H. Koinuma and Y. Segawa, *Solid State Commun.* **103**, 459 (1997).

[6] B. W. Thomas and D. Walsh, *Electronics Lett.* **9**, 362 (1973).

[7] T. Minami, M. Tanigawa, M. Yamanishi and T. Kawamura, *Jpn. J. Appl. Phys.* **13**, 1475 (1974).

[8] I. T. Drapak, *Soviet Phys. Semiconductors* **2**, 513 (1968). (The electro-luminescence from Cu_2O/ZnO was stated from p-n junction. However, judging from high bias voltage required for the emission, it has been rather considered to be due to insulator-semiconductor junction.)

[9] T. Aoki, Y. Hatanaka and D. C. Look, *Appl. Phys. Lett.* **76**, 3257 (2000).

[10] M. Joseph, H. Tabata and T. Kawai, Jpn. *J. Appl. Phys.* **38**, L1205 (1999).

[11] H. Kawazoe, M. Yasukawa, H. Hyodo, M. Kurita, H. Yanagi and H. Hosono, *Nature (London)* **389**, 939 (1997).

[12] H. Yanagi, S. Inoue, K. Ueda, H. Kawazoe qnd H. Hosono, *J. Appl. Phys.* **88**, 4159 (2000).

[13] A. Kudo, H. Yanagi, H. Hosono and H. Kawazoe, *Appl. Phys. Lett.* **73**, 220 (1998).

[14] H. Ohta, K. Kawamura, M. Orita, M. Hirano, N. Sarukura, and H. Hosono, *Appl. Phys, Lett.* 77, 475 (2000).

[15] H. Ohta, M. Orita, M. Hirano, H. Tanji, H. Kawazoe and H. Hosono, *Appl. Phys. Lett.* **76**, 2740 (2000).

[16] H. Ohta, H. Tanji, M. Orita, H. Hosono and H. Kawazoe, *Mat. Res. Soc. Symp. Proc.* **570**, 309 (1999).

[17] J. M. Hvam, *Phys. Status. Solidi* **B 63**, 511 (1974).

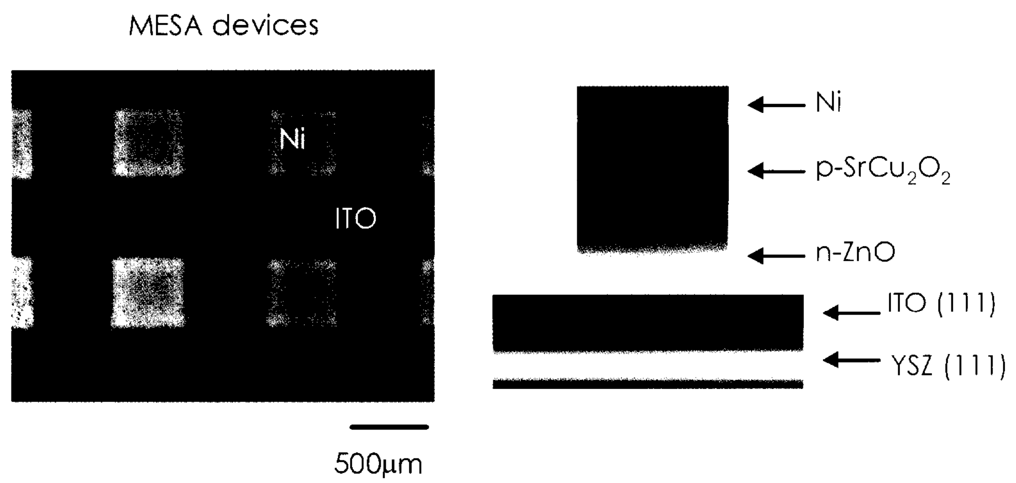

Figure 6-1. Schematic illustration (right) and photograph (left) of the LED. ITO and Ni are used as n- and p-electrodes, respectively.

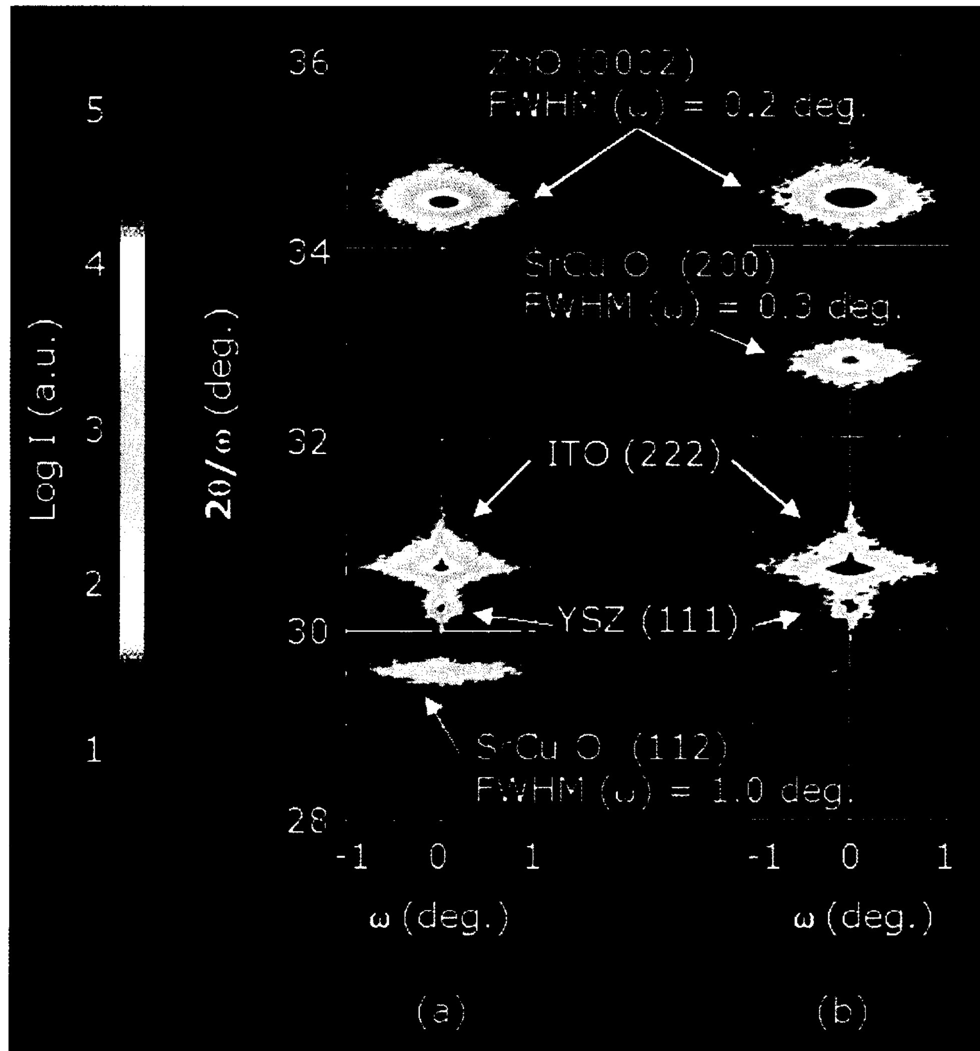

Figure 6-2. Out-of-plane XRD reciprocal-space mappings of multi-layered films of Ni / $SrCu_2O_2$ / ZnO / ITO deposited on YSZ (111) substrate. Growth temperature of $SrCu_2O_2$ of film A and B were (a) 350 °C and (b) 600 °C, respectively.

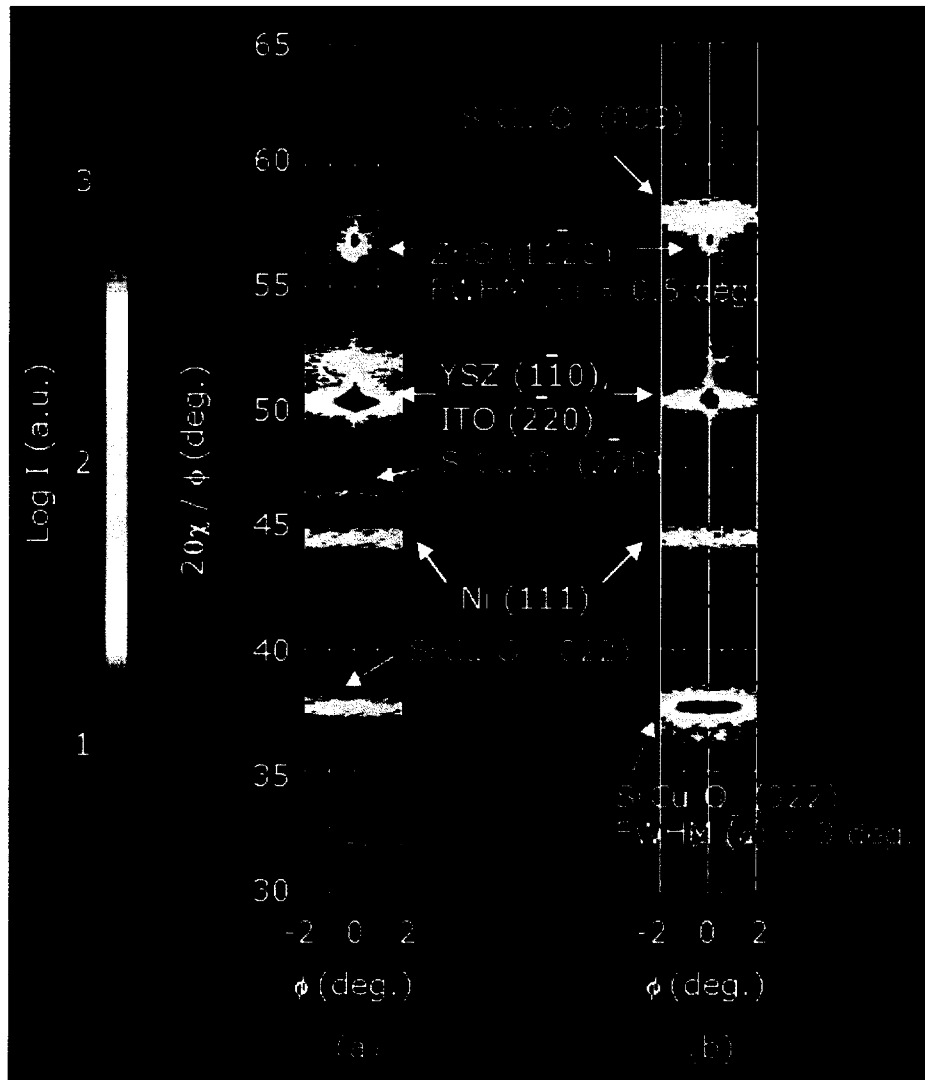

Figure 6-3. In-plane XRD reciprocal-space mappings of multi-layered films of Ni / $SrCu_2O_2$ / ZnO / ITO deposited on YSZ (111) substrate. Growth temperature of $SrCu_2O_2$ of film A and B were (a) 350 °C and (b) 600 °C, respectively.

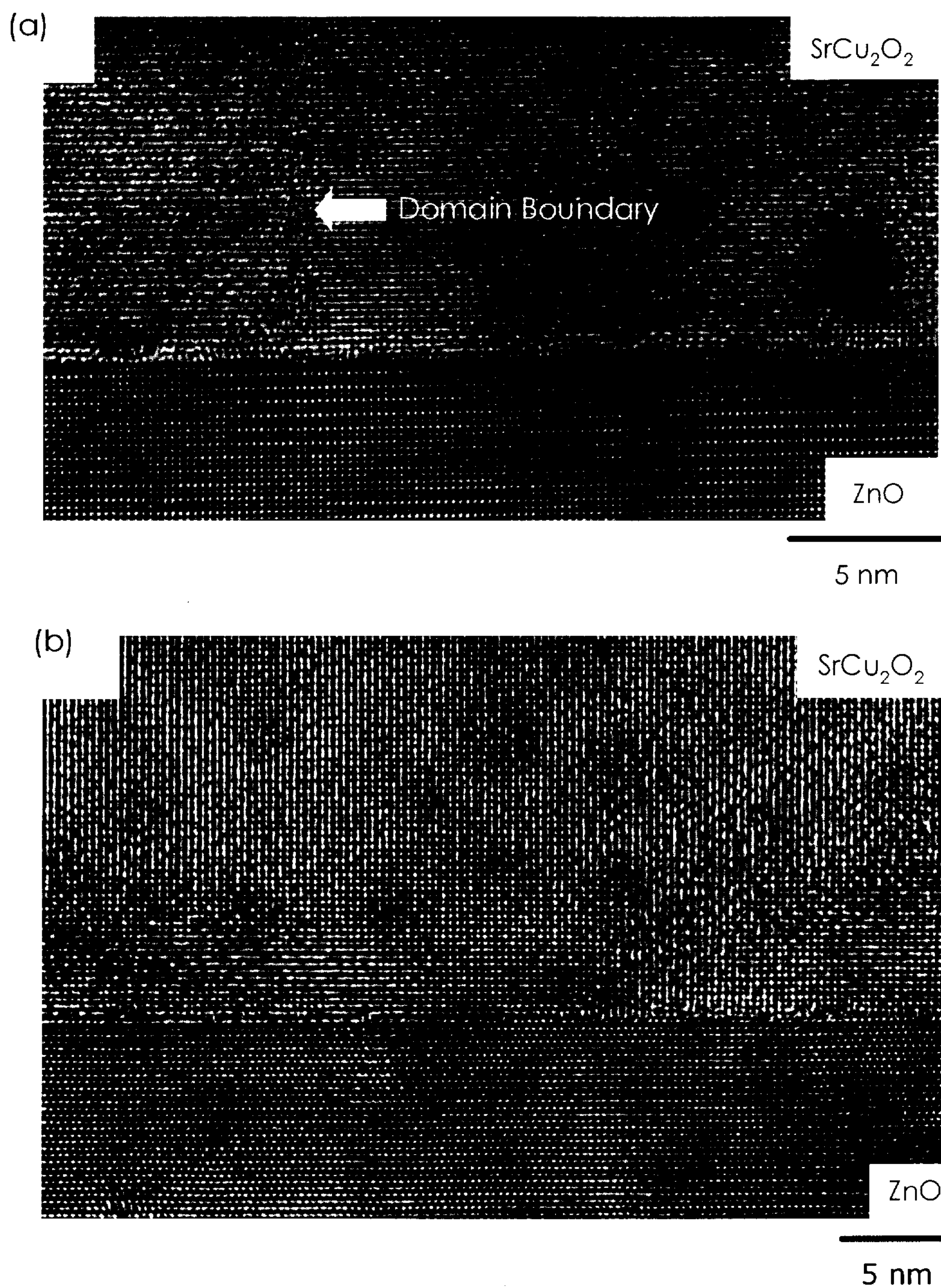

Figure 6-4. Cross-sectional HR-TEM images near the p-n heterojunction, $SrCu_2O_2$ (top) / ZnO (bottom). Growth temperature of $SrCu_2O_2$ of film A and B were (a) 350 °C and (b) 600 °C, respectively.

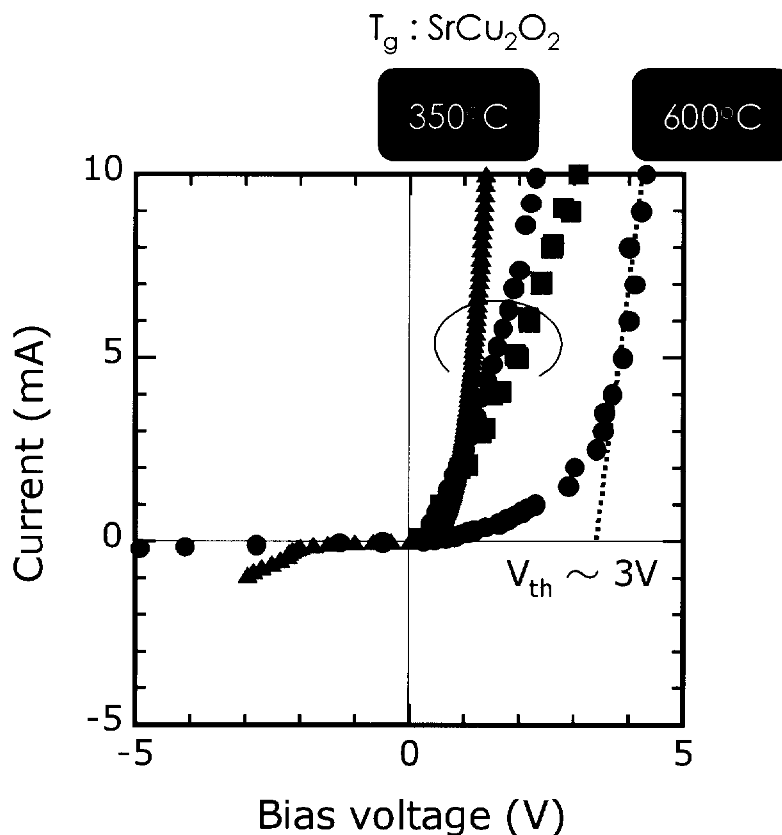

Figure 6-5. Typical I-V characteristics of fabricated diodes composed of p-$SrCu_2O_2$ / n-ZnO heterojunction (▲, ●, ■: LED A, ●: LED B). The LED A and B, which were prepared using film A and B, respectively, exhibited rectifying I-V characteristics inherent to p-n heterojunction. The I-V curves of LED A (▲, ●, ■) fluctuated considerably from sample to sample, while those of LED B did not scatter so much.

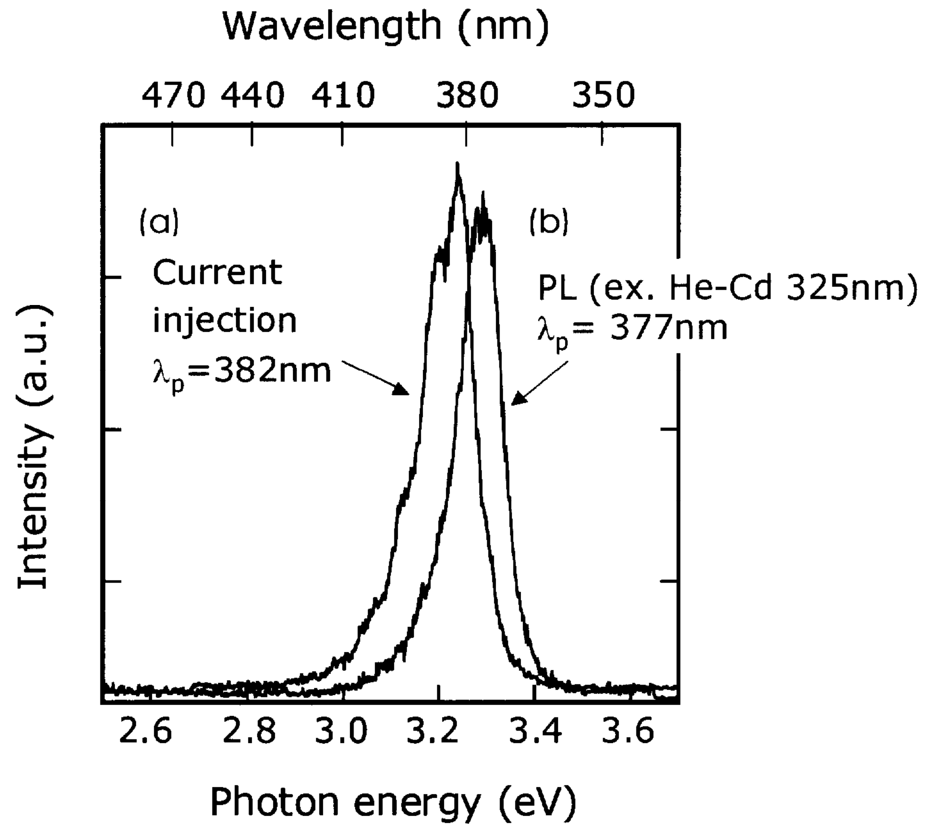

Figure 6-6. UV emission spectrum of p-$SrCu_2O_2$ / n-ZnO p-n junction LED. (a) EL: emission due to current injection, (b) PL: photoluminescence excited with 325 nm He-Cd laser light

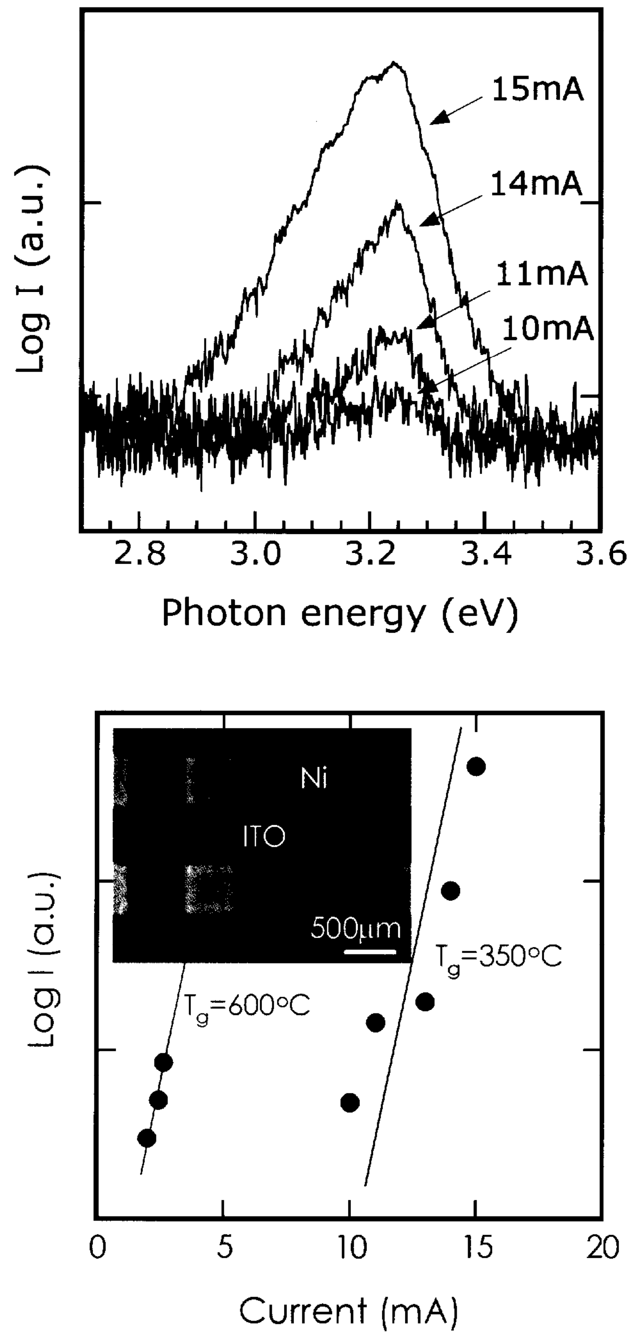

Figure 6-7. UV emission spectra of the p-$SrCu_2O_2$ / n-ZnO junction LED A (a) and B (b) for several currents. Growth temperature of $SrCu_2O_2$ of LED A and B were (a) 350 °C and (b) 600 °C, respectively.

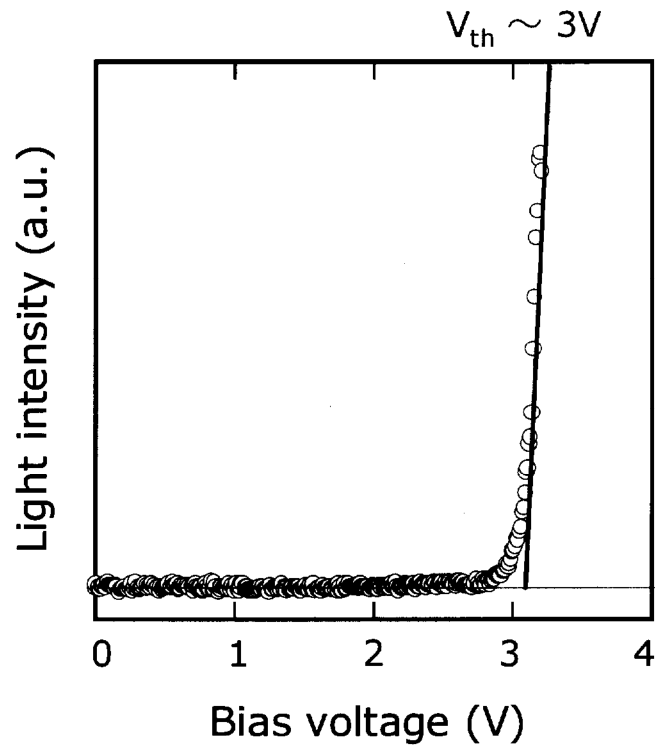

Figure 6-8. Emission intensity of LED B as a function of bias voltage. The turn-on voltage is about 3 V.

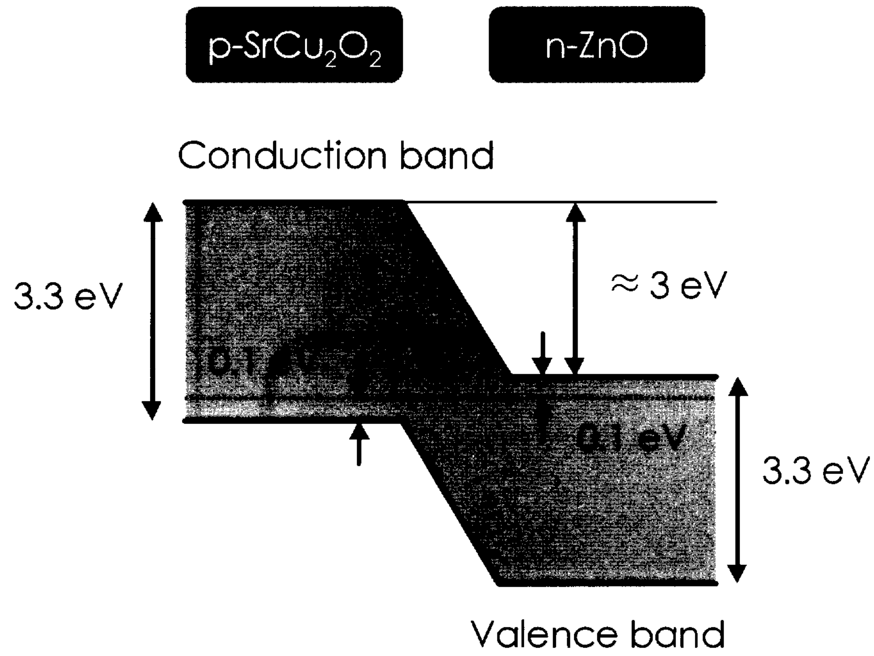

Figure 6-9. Schematic band lineup of p-$SrCu_2O_2$ and n-ZnO.

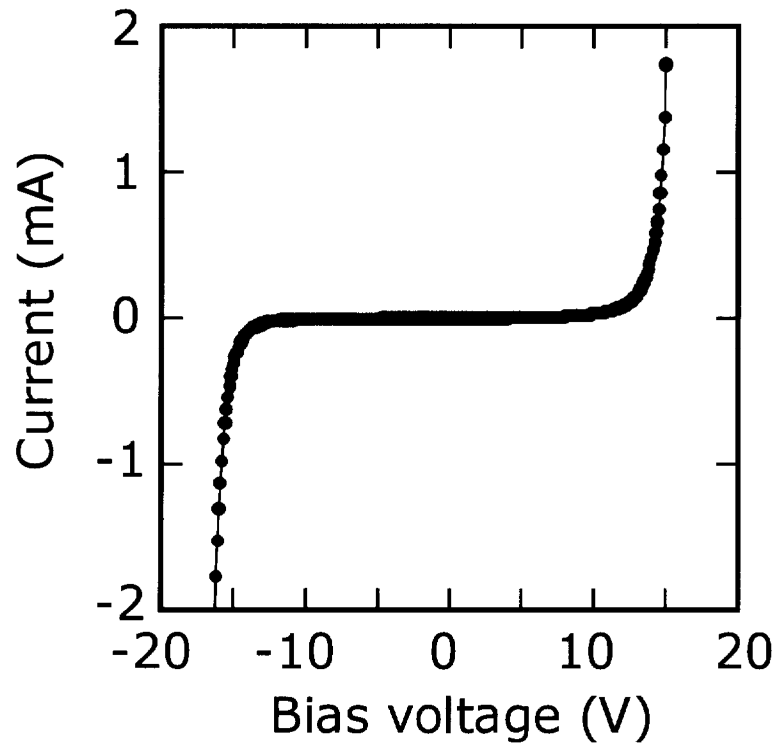

Figure 6-10. I-V characteristic of fabricated diode composed of p-$SrCu_2O_2$ / i-ZnO / n-ZnO heterojunction (LED C). Film C was obtained with the same condition as film B, except the higher laser irradiation energy density onto target.

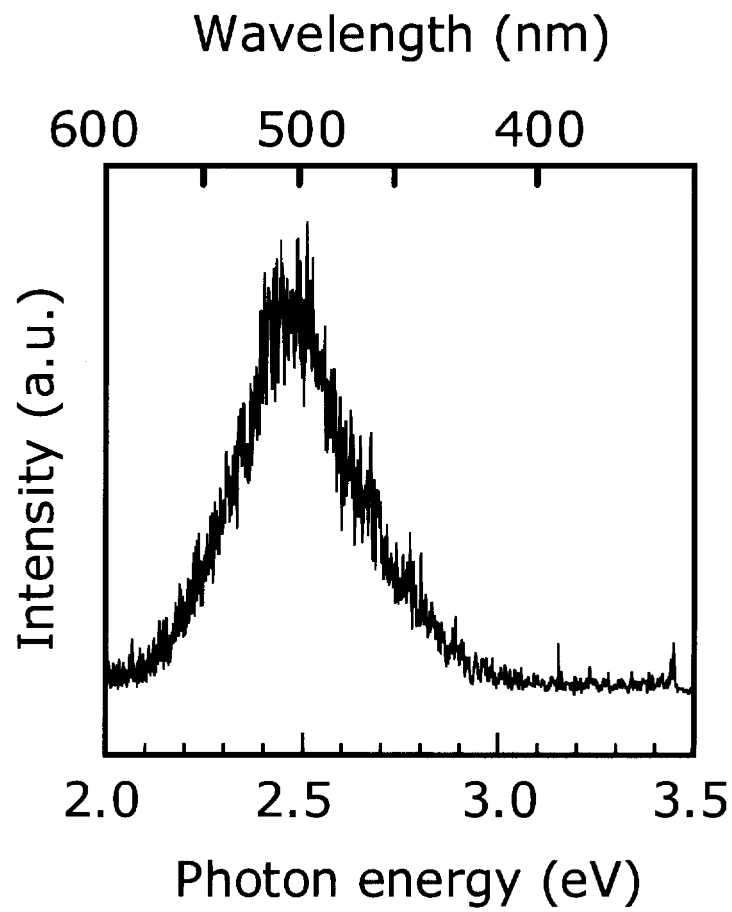

Figure 6-11. Visible emission spectrum of LED C

Chapter 7.
Summary and General Conclusions

7.1. Conclusions

UV-emitting diode operating at room temperature was realized in the present study for the first time using a p-n heterojunction composed of transparent oxide semiconductors, p-$SrCu_2O_2$ and n-ZnO. In the process to realize the UV-LED, high quality epitaxial thin films of ITO and ZnO were successfully grown by PLD technique on YSZ (111) single crystal substrate. Electronic structure and optical properties of p-type transparent oxide semiconductor, $SrCu_2O_2$, were investigated and found whose band gap was direct-forbidden type. The results of present study are summarized as follows:

In chapter 2, High quality ITO thin films were grown hetero-epitaxially on extremely flat substrate of (001) YSZ by a pulsed laser deposition technique at a substrate temperature of 600°C. The crystal orientation relationship between the film and YSZ were confirmed as ITO (001) // YSZ (001) and ITO (010) // YSZ (010), respectively, by HR-XRD and HR-TEM. The carrier densities of the films were almost equal to SnO_2 concentration in the films. That is, almost all the doped Sn^{4+} ions were activated to release electrons to the conduction band. The carrier densities of the films were enhanced up to 1.9×10^{21} cm^{-3}, while the Hall mobility showed a slight, almost linear, decrease from 55 to 40 $cm^2V^{-1}s^{-1}$ with increasing SnO_2 concentration. The low resistivity is due to larger electron mobility, which most likely resulted from good crystal quality of the films. The optical transmissivity of the film exceeded 85% at wavelengths from

340 to 780 nm.

In chapter 3, Highly electrical conductive (resistivity: ~1 x 10^{-4} Ωcm) indium-tin-oxide films were grown heteroepitaxially on YSZ (111) and (100) surfaces at a substrate temperature of 900 °C by a pulsed laser deposition method, and crystal quality and surface morphology of the films were evaluated by using high-resolution X-ray diffraction and atomic force microscope. Higher growth temperature, use of cleaved surface as a substrate and an increase in oxygen pressure are essential to fabricate ITO thin film with atomically flat surface. The full width at half maximum of out-of-plane X-ray rocking curves of ITO (111) grown on YSZ (111) and ITO (400) on YSZ (100) surface were 54 and 720 arcsecond, respectively, which indicates ITO (111) films exhibited higher crystal quality compare to ITO (100) films. ITO film was basically grown on YSZ (111) by 3D-spiral growth mode with flat terraces and steps corresponding to (222) plane spacing of 0.29 nm, and the grain size was decreased with increasing oxygen pressure during ITO film growth to improve overall surface flatness, while only columnar structure was observed in the ITO (100) film surface.

In chapter 4, Heteroepitaxial films of ZnO were grown on the (111) surface of YSZ and sapphire (0001) by the PLD method, using KrF eximer laser (248 nm) in an ultra-high-vacuum chamber at 600 °C. The epitaxial relationship between the ZnO/YSZ interface is ZnO [$11\bar{2}0$]//YSZ [$1\bar{1}0$]. FWHM of the ZnO (0002) rocking curve of the ZnO/YSZ and ZnO/sapphire were 0.12 ° and 1.7 °, respectively. Cross-sectional TEM images suggested that ZnO on sapphire produced relatively larger amounts of twisted columns as compared to ZnO on YSZ. The Hall mobility of ZnO/sapphire was 7 cm^2/Vs,

which was less than that of ZnO/YSZ (45 cm^2/Vs). Judging from these results, conduction carrier would be scattered at the boundaries of the twisted columns. The surface of heteroepitaxial ZnO film deposited at 800 °C was composed of hexagonally shaped grains. Flat terraces and step structures were observed in individual ZnO grains, and the step height between terraces was about 0.5 nm, which was good in agreement with the lattice constant of c-axis of ZnO (0.52 nm). The grain size of ZnO increased with film thickness, while Hall mobility of ZnO/YSZ increased from 10 cm^2/Vs to 75 cm^2/Vs.

In chapter 5, The electronic structure of wide gap (~3.3 eV) p-type oxide semiconductor, $SrCu_2O_2$, was examined by photoelectron and optical spectroscopy, and results were compared with energy band structure calculated by local density approximation method to clarify the origin of p-type conductivity in this material. The basic electronic structure around the band gap region was found to be quite similar to that of Cu_2O, despite a considerably large difference in the band gap energy. That is, the mixed orbital between 3d and 4sp of Cu^+ ion is hybridized with 2p orbital of ligand O^{2-} ions due to a sizable covalent contribution of Cu - O bonds, to constitute the valence band maximum. While, the conduction band minimum is dominantly composed of the hybridized orbital of Cu 4sp and O2p, forming the direct band gap at Γ point. A sharp absorption band was observed near the fundamental absorption edge likely attributed to exciton. Although the corresponding exciton emission was not observed near the absorption edge, a blue-green emission band (Stokes shift of ~1 eV) was observed at ~2.47 eV. The emission is presumably attributed to intra-atomic transition of Cu^+, partially allowed by p-orbital mixing into s- and d-orbital.

In chapter 6, A UV light-emitting diode was realized using a p-n heterojunction composed of the transparent conductive oxides p-$SrCu_2O_2$ and n-ZnO. A Ni/$SrCu_2O_2$/ZnO/ITO multi-layered film was epitaxially grown on an extremely flat YSZ (111) surface by a pulsed-laser deposition technique. $SrCu_2O_2$ (112) was preferentially grown on ZnO (0001) at 350 °C, while the preferential plane was changed into the (100) when the temperature was increased to 600 °C. The grown films were processed by conventional photolithography followed by reactive ion etching to fabricate heterojunction diodes. The resulting devices exhibited rectifying I-V characteristics inherent to p-n junctions. A relatively sharp electro-luminescence band centered at 382 nm, attributed to transitions associated with exciton-exciton collision or electron-hole plasma in ZnO, was generated by applying a forward bias voltage greater than the turn-on voltage of 3 V. UV-LED performance characteristics such as threshold current and conversion efficiency improved with higher $SrCu_2O_2$ deposition temperatures. On the other hand, increased laser power density at 600 °C during deposition raised the incidence of insulating layer formation between the p and n layers, probably due to migration of K^+ ions doped as an acceptor impurity. The resulting p-i-n diode emits broad luminescence centered at 500 nm for forward voltage greater than 14 V.

9.2. Suggested Future Research

In the present study, active diode composed of "hetero" junction of oxide was realized by heteroepitaxial growth of p-$SrCu_2O_2$ on n-ZnO. Lattice mismatch between p-$SrCu_2O_2$ (112) on n-ZnO (0001) is as large as 13 %, which is much larger than that of

typical compound semiconductors. Although lattice mismatch is key factor for epitaxial growth of compound semiconductors, heteroepitaxial growth occurs independently in lattice mismatch in case of oxide semiconductors. Because oxide semiconductors are ionic bond crystal. Heterojunction is effective to fabricate optoelectronic devices with oxide semiconductors. When a suitable combination of oxide semiconductors is used, optoelectronic device showing good performance beyond compound semiconductors may be realized.

Very recently, H. Yanagi and Co-workers reported p-n "homo" junction diode of transparent oxide semiconductor of $CuInO_2$ [1]. Although the diode was fabricated using polycrystalline film of $CuInO_2$, rectifying property was observed.

K. Ueda and Co-workers reported novel p-type transparent oxy-sulfide semiconducting thin film, LaCuOS [2], which emits near-UV light due to excitons by excitation of UV-laser even at room temperature. The film was polycrystal grown on SiO_2 glass substrate by R.F. sputtering technique. The energy band structure of LaCuOS was also reported by K. Ueda and Co-workers [3]. Band gap of LaCuOS is direct transition type and the transition form valence band maximum to conduction band minimum was optically allowed. Thus, LaCuOS is promising candidate active material for optoelectronic device.

In the present study, ITO thin films with extremely flat surface were grown on YSZ (111) surface, whose surface was composed of atomically flat terraces (terrace width$\sim$100 nm) and steps of 0.3 nm. If the ITO thin film is applied to transparent conductive substrate for STM observation of organic phosphors, i.e. DNA, STM image and tunnel electron luminescence of the phosphors would be observed at same time.

References

[1] H. Yanagi, K. Ueda, H. Hosono, H. Ohta, M. Orita and M. Hirano, *Appl. Phys. Lett.* (Submitted).

[2] K.Ueda, S.Inoue, H.Kawazoe and H.Hosono, *Appl. Phys. Lett.* **77**, 2701 (2000).

[3] K.Ueda, S.Inoue, H.Hosono, N.Sarukura and M.Hirano, *Appl. Phys. Lett.* **78**, 2333 (2001).

Acknowledgements

The present study was carried out under the guidance of Professor Hideo Hosono, Professor Hiroshi Kawazoe (who retired in 1999, Research fellow, HOYA Co.) and Research Associate Kazushige Ueda of Tokyo Institute of Technology from October 1998 to September 2001.

I would like to express my sincere thanks to Professor Hideo Hosono, Professor Hiroshi Kawazoe and Research Associate Kazushige Ueda for their kind guidance and a number of important suggestions.

I wish to express my gratitude to Professor Youtaro Yamazaki, Professor Takahiro Seki, Professor Mamoru Yoshimoto and Professor Hiroshi Funakubo of Tokyo Institute of Technology for their critical regarding of this thesis and for their valuable comments.

I wish to thank Research manager Masahiro Hirano, Dr. Masahiro Orita, Dr. Nobuhiko Sarukura, Dr. Ken-ichi Kawamura and other members of Hosono Transparent ElectroActive Materials, ERATO, JST for their discussion and experimental help.

I wish to thank Dr. Hiroshi Yanagi and other members of Hosono laboratory for their discussion and experimental help.

I also wish to thank my wife Naomi and my daughter Aoi for great care of my research life.

Finally, I deeply appreciate my parents, Katsumi and Michiko Ohta, wish all my heart. Special thanks for giving me a chance to study.

Hiromichi Ohta

Publication Lists

Papers included in the thesis

1. "Fabrication and characterization of ultraviolet-emitting diode composed of transparent p-n heterojunction, p-$SrCu_2O_2$ and n-ZnO", **H. Ohta**, M. Orita, M. Hirano, H. Hosono, *J. Appl. Phys.* **89**, 5720 (2001).

2. "Current injection emission from a transparent p-n junction composed of p-$SrCu_2O_2$ / n-ZnO", **H. Ohta**, K. Kawamura, M. Orita, N. Sarukura, M. Hirano and H. Hosono, *Appl. Phys. Lett.*, **77**, 475 (2000).

3. "UV-emitting diode composed of transparent oxide semiconductors: p-$SrCu_2O_2$ / n-ZnO", **H. Ohta**, K. Kawamura, M. Orita, N. Sarukura, M. Hirano and H. Hosono, *Electronics Letters*, **36**, 984 (2000).

4. "Fabrication and near-UV emission of p-$SrCu_2O_2$ / n-ZnO heterojunction LED", **H. Ohta**, M. Orita, M. Hirano and H. Hosono, *J. Sur. Sci. Jpn.* **22**, 419 (2001). (in Japanese).

5. "Fabrication and current injection UV-light emission from a transparent p-n heterojunction composed of p-$SrCu_2O_2$ and n-ZnO", **H. Ohta**, M. Orita, M. Hirano and H. Hosono, *Asian Ceramic Science for Electronics I* (to be published).

6. "Near UV-emitting diodes based on transparent P-N junction composed of heteroepitaxially grown p-$SrCu_2O_2$ and n-ZnO", H. Hosono, **H. Ohta**, K. Hayashi, M. Orita and M. Hirano, *J. Crystal Growth* (accepted).

7. "Frontier of transparent conductive oxide thin films", H. Hosono, M. Orita, **H. Ohta**, K. Ueda and M. Hirano, *Vacuum* (accepted).

8. "Electronic structure and optical properties of p-type transparent oxide semiconductor; $SrCu_2O_2$", **H. Ohta**, M. Orita, M. Hirano, I. Yagi, K. Ueda and H. Hosono, *J. Appl. Phys.* (submitted).

9. "Epitaxial growth of transparent conductive oxides", **H. Ohta**, M. Orita, M. Hirano, K. Ueda and H. Hosono, *International Journal of Modern Physics B* (to be published).

10. "Transparent conducting indium-tin-oxide thin film with extremely flatted surface", **H. Ohta**, M. Orita, M. Hirano, H. Hosono, *Mat. Res. Soc. Symp. Proc.* (to be published).

11. "Highly electrically conductive indium-tin-oxide thin films epitaxially grown on yttria-stabilized zirconia (100) by pulsed-laser deposition", **H. Ohta**, M. Orita, M. Hirano, H. Tanji, H. Kawazoe and H. Hosono, *Appl. Phys. Lett.*, **76**, 2740 (2000).

12. "Low electrically resistive transparent indium-tin-oxide epitaxial film on (001)

surface of YSZ by pulsed laser deposition", **H. Ohta**, M. Orita, M. Hirano, H. Hosono, H. Kawazoe and H. Tanji, *Mat. Res. Soc. Symp. Proc.* **Vol.623**, 253 (2000).

13. "Heteroepitaxial growth of zinc oxide single crystal thin films on (111) plane YSZ by pulsed laser deposition", **H. Ohta**, H. Tanji, M. Orita, H. Hosono and H. Kawazoe, *Mat. Res. Soc. Symp. Proc.* **Vol.570**, 309 (1999).

Other Papers

1. "Amorphous transparent conductive oxide $InGaO_3(ZnO)_m$ (m<4) : a Zn 4s Conductor", M. Orita, **H. Ohta**, M. Hirano, S. Narushima and H. Hosono, *Phil. Mag.* **81**, 501 (2001).

2. "Epitaxial growth of transparent p-type conducting $CuGaO_2$ thin films on sapphire (001) substrates by pulsed laser deposition", K. Ueda, T. Hase, H. Ynagai, H. Kawazoe, H. Hosono, **H. Ohta**, M. Orita and M. Hirano, *J. Appl. Phys.* **89**, 1790 (2001).

3. "Pulsed laser deposition system for producing oxide thin films at high temperature", M. Orita, **H. Ohta**, H. Hiramatsu, M. Hirano, S. Den, M. Sasaki, T. Katagiri, H. Minura and H. Hosono, *Rev. Sci. Inst.* **72**, 3340 (2001).

4. "Fabrication of all oxide transparent p-n homojunction using bipolar $CuInO_2$", H. Yanagi, K. Ueda, H. Hosono, **H. Ohta**, M. Orita and M. Hirano, *Appl. Phys. Lett.*

(submitted).

5. "Properties of a novel amorphous transparent conductive oxide, $InGaO_3(ZnO)_m$", M. Orita, **H. Ohta**, M. Hirano, H. Hosono, K. Morita, H. Tanji and H. Kawazoe, *Mat. Res. Soc. Symp. Proc.* **Vol. 623**, 291 (2000).

6. "Heteroepitaxial growth of In_2O_3 on YSZ (100) single crystal surface", M. Orita, **H. Ohta**, H. Tanji, H. Hosono and H. Kawazoe, *Mat. Res. Soc. Symp. Proc.* **Vol. 558**, 399 (2000).

7. "Deep-ultraviolet transparent conductive β-Ga_2O_3 thin films", M. Orita, **H. Ohta**, M. Hirano and H. Hosono, *Appl. Phys. Lett.* 77, 4166 (2000).

8. "Thermoelectirc properties of $(ZnO)_5In_2O_3$ thin films prepared by r.f. sputtering method", H. Hiramatsu, **H. Ohta**, W. S. Seo and K. Koumoto, *J. Jpn. Soc. Powder and Powder Metal.* **44**, 44 (1997).

9. "Thermoelectirc properties of homologous compounds in the ZnO-In_2O_3 system", **H. Ohta**, W. S. Seo and K. Koumoto, *J. Amer. Ceram. Soc.* 79, 2193 (1996).

Reviews

1. "Development of near-UV-emitting diode using transparent oxide semiconductors", **H. Ohta**, M. Orita, M. Hirano and H. Hosono, *Bull. Ceram. Soc. Japan* **36**, 285

(2001) (in Japanese).

2. "Recent advantages of transparent conductive oxides", M. Orita, **H. Ohta** and H. Hosono, *Hyomen (Surface)* **38**, 344 (2000) (in Japanese).

3. "UV-LED composed of p-$SrCu_2O_2$ / n-ZnO heterojunction realized for the first time", **H. Ohta**, M. Orita, M. Hirano and H. Hosono, *285th Keikoutaidougakkai Kouenyokou*, 17 (2000) (in Japanese).

Oral Presentation Lists

International

1. "Epitaxial Growth of Transparent Conductive Oxides", **H. Ohta**, M. Orita, K. Ueda, M. Hirano, and H. Hosono, Intl Conference on Materials for Advanced Technologies ICMAT 2001 MRS-Singapore, Singapore, Singapore July 1-6, 2001. (Invited)

2. "Improvement of UV-Light Emission for P-N Heterojunction LED Composed of p-$SrCu_2O_2$ AND n-ZnO", **H. Ohta**, M. Orita, M. Hirano and H. Hosono, 2001 MRS Spring Meeting, San Francisco, USA, April 16-20, 2001. (Invited)

3. "Fabrication and Current Injection UV-Light Emission From a Transparent p-n Heterojunction Composed of p-$SrCu_2O_2$ and n-ZnO", **H. Ohta**, M. Orita, M. Hirano and H. Hosono, The 1st Asian Meeting on Electroceramics, Kawasaki, Japan, October 26-27, 2000.

4. "Room Temperature Operation of UV-LED Composed of TCO Hetero P-N Junction, p-$SrCu_2O_2$ / n-ZnO", **H. Ohta**, K. Kawamura, M. Orita, N. Sarukura, M. Hirano and H. Hosono, 2000 MRS Spring Meeting, San Francisco, USA, April 24-28, 2000.

5. "A Very Low Electrical Resistive Transparent Indium-Tin-Oxide Epitaxial Film on (100) Surface of YSZ by Pulsed Laser Deposition", **H. Ohta**, M. Orita, H. Tanji, H.

Kawazoe, M. Hirano and H. Hosono, 2000 MRS Spring Meeting, San Francisco, USA, April 24-28, 2000.

6. "Heteroepitaxial Growth of In_2O_3 on YSZ (100) Surface by Pulsed Laser Deposition", **H. Ohta**, H. Tanji, M. Orita, H. Kawazoe and H. Hosono, International Workshop on Optoelectronic Oxides: Materials and Processing, Tokyo, Japan, July 23, 1999.

Domestic

1. "Ultraviolet Emitting Diode Composed of P-N Heterojunction for Transparent Oxide Semiconductors", **H. Ohta**, M. Orita, M. Hirano and H. Hosono, The 12th Meeting on Glass for Photonics, Tokyo, Japan, August 2001. (Invited)

2. "Room temperature UV-emission from transparent oxide p-n heterojunction by current injection", **H. Ohta**, M. Orita and M. Hirano, The 48th Spring Meeting 2001 (Symposium), The Japan Society of Applied Physics and Related Societies, Tokyo, Japan, March 2001. (Invited)

3. "Fabrication of Atomically Flat ITO Thin Film and Application for UV-LED Composed of P-$SrCu_2O_2$ / N-ZnO", **H. Ohta**, M. Orita, M. Hirano and H. Hosono, The 20th Meeting of the Surface Science Society of Japan, Tokyo, Japan, November 2000.

4. "UV-LED Composed of p-$SrCu_2O_2$ / n-ZnO Heterojunction Realized for the First Time", **<u>H. Ohta</u>**, M. Orita, M. Hirano and H. Hosono, 285th Keikoutaidougakkai Kouenkai, Tokyo, November 24, 2000. (Invited)

5. "Hetero-epitaxial growth of p-$SrCu_2O_2$ layer on n-ZnO layer and improvement of characteristics for UV-LED", **<u>H. Ohta</u>**, M. Orita, M. Hirano and H. Hosono, The 61th Autumn Meeting 2000, The Japan Society of Applied Physics and Related Societies, Sapporo, Japan, September 2000.

6. "ITO thin film with atomically flatted surface", **<u>H. Ohta</u>**, M. Orita, M. Hirano and H. Hosono, The 61th Autumn Meeting 2000, The Japan Society of Applied Physics and Related Societies, Sapporo, Japan, September 2000.

7. "Fabrication and luminescence of wide band gap p-n junction LED, p-$SrCu_2O_2$ / n-ZnO", **<u>H. Ohta</u>**, M. Orita, K. Kawamura, N. Sarukura, M. Hirano and H. Hosono, The 47th Spring Meeting 2000, The Japan Society of Applied Physics and Related Societies, Tokyo, Japan, March 2000.

8. "Very low resistive ITO thin films epitaxially grown on YSZ (100) by PLD method", **<u>H. Ohta</u>**, M. Orita, H. Tanji, H. Kawazoe, M. Hirano and H. Hosono, The 47th Spring Meeting 2000, The Japan Society of Applied Physics and Related Societies, Tokyo, Japan, March 2000.